Impact of assimilating a merged sea ice thickness from CryoSat-2 and SMOS in the Arctic reanalysis

Jiping Xie[1], François Counillon[1, 2], and Laurent Bertino[1, 2]

1. *Nansen Environmental and Remote Sensing Center, Bergen N5006, Norway*
2. *Bjerknes Center for Climate Research, Bergen, Norway*

*Corrsponding author: Jiping Xie, E-mail: jiping.xie@nersc.no

Abstract

Forecasting accurately the Sea Ice Thickness (SIT) in the Arctic is a major challenge. The new SIT product (referred to as CS2SMOS) merges measurements from the CryoSat-2 and SMOS satellites on a weekly basis during the winter. The impact of assimilating CS2SMOS data is tested for the TOPAZ4 system - the Arctic component of the Copernicus Marine Environment Monitoring Services (CMEMS). TOPAZ4 currently assimilates a large set of ocean and sea ice observations with the Deterministic Ensemble Kalman Filter (DEnKF).

Two parallel reanalyses are conducted without (Official run) and with (Test run) assimilation of CS2SMOS data from 19th March 2014 to 31st March 2015. Since only mapping errors were provided in the CS2SMOS observation, an arbitrary term was added to compensate for the missing errors, but was found a posteriori too large. The SIT bias (too thin) is reduced from 16 cm to 5 cm and the standard errors decrease from 53 cm to 38 cm (by 28%) when compared to the assimilated SIT. When compared to independent SIT observations, the error reduction is 24% against the Ice Mass Balance (IMB) buoy 2013F and by 12.5% against SIT data from the IceBridge campaigns. The improvement of sea ice volume persists through the summer months in the absence of CS2SMOS data. Comparisons to sea ice drift from satellite show that dynamical adjustments reduce the drift errors around the North pole by about 8-9% in December 2014 and February 2015. Finally, using the Degrees of Freedom for Signal (DFS), we find that CS2SMOS makes the prime source of information in the central Arctic and in the Kara Sea. We therefore recommend the assimilation of C2SMOS for Arctic reanalyses in order to improve the ice thickness and the ice drift.

Keywords: Sea ice thickness; Arctic reanalysis; CS2SMOS; EnKF; observing systems evaluation;

1. Introduction

Sea ice plays an important role in the Arctic climate system because it prevents the rapid exchange of heat flux between the ocean and atmosphere. A decline and a thinning of the sea ice cover has occurred in the past decades (e.g. Johannessen et al., 1999; Comiso et al., 2008; Stroeve et al., 2012) as well as an increase of deformation rates and drift speed (Rampal et al. 2009). It is expected that these changes will have significant impacts on the Arctic Ocean Circulation (e.g. Levermann et al., 2007; Budikova, 2009; Kinnard et al., 2011) and on the future human living environment (Schofield et al., 2011; Bathiany et al., 2016). The interpretation of such changes is severely hampered by the sparseness of observations, therefore the reanalyses that can provide continuous spatio-temporal reconstructions by assimilating existing observations into dynamical models have become increasingly popular tools. In addition, recent studies (Day et al. 2014; Guemas et al., 2014; Melia et al. 2015) have shown that SIT anomalies play an important role for the Arctic predictability up to seasonal time scale.

Satellite observations of sea ice concentration (SIC) have been available since 1979 and have allowed an accurate monitoring of sea ice extent (SIE) during that period. Data assimilation of SIC has constrained the position of the sea ice edge (Lisæter et al., 2003; Stark et al., 2008; Posey et al., 2015), but large disagreements (e.g., Uotila et al, 2018) remain in the estimation of sea ice volume because observations of sea ice thickness (SIT) are very incomplete.

Until the 1990s, the only SIT measurements were sparse in situ measurements and submarine data. With new satellites, continuous estimates of SIT on basin scale have been achieved using satellite radar and laser altimeters: European Remote Sensing (ERS), Envisat and the NASA Ice, Cloud and land Elevation Satellite (ICESat). These were used to document the rapid thinning of sea ice in Arctic (Laxon et al., 2003; Kwok and Rothrock, 2009).

CryoSat-2, launched in April 2010, has been the first satellite dedicated to measure with high accuracy the sea ice freeboard, from which SIT can be derived (Ricker et al., 2014; Tilling et al., 2016). However, the resulting SIT estimates are still very uncertain because of uncertainties in the snow depth (using climatology), snow penetration and sea ice density (Kern et al, 2015; Khvorostovsky and Rampal, 2016). Those uncertainties are large for thin ice

(<1 m). In parallel, satellite measurements from a passive microwave radiometer have retrieved SIT of thin ice (Martin et al., 2004; Heygster et al., 2009) from the Soil Moisture and Ocean Salinity (SMOS) satellite brightness temperature in the L-Band microwave frequency (1.4 GHz) (Kaleschke et al., 2010; Tian-Kunze et al., 2014). Although the consistency between the SMOS and CryoSat-2 estimates is still poor (X. Wang et al., 2016), a recent initiative has combined the two data sets in the Arctic (e.g. Kaleschke et al., 2015; Ricker et al., 2017) into a merged weekly SIT from the CryoSat-2 altimeter and SMOS radiometer (referred to as CS2SMOS, available online at http://www.meereisportal.de). The usefulness of assimilating this data set for reanalysis and operational forecasting needs to be tested.

In this study, the CS2SMOS will be assimilated into the TOPAZ4 forecast system, which is a coupled ocean-sea ice data assimilation system using the Deterministic Ensemble Kalman Filter (DEnKF; Sakov and Oke, 2008). The Ensemble Kalman Filter has previously been demonstrated for assimilation of SIT data (Lisæter et al., 2007) of freeboard data (Mathiot et al., 2012) and of the CS2SMOS data (Mu et al., 2018) as well. TOPAZ4 is the Arctic Marine Forecasting system in the Copernicus Marine Environment Monitoring Services (CMEMS, http://marine.copernicus.eu). Every day, it publishes a 10-day forecast of the ocean physics and biogeochemistry in the Arctic through the CMEMS portal. It also provides a long reanalysis from 1990 to the present – currently 2016 - that is extended every year. This reanalysis has been widely used and validated (Ferreira et al., 2015; Johannessen et al., 2014; Xie et al., 2017). Although SIT products are so far not assimilated into the TOPAZ4 reanalysis, the Arctic SIT distribution in TOPAZ4 shows some degree of spatial coherency with that of ICESat in spring and autumn of 2003-2008: it underestimates SIT (up to 1 m) north of Canadian Arctic Archipelago and Greenland and overestimates it by approximately 0.2 m in the Beaufort Sea (Xie et al., 2017). Even though the SIT from ICESat has been reported too thick by about 0.5 m (Lindsay and Schweiger, 2015), the SIT from TOPAZ4 undoubtedly has spatial biases. Similar biases for SIT have been reported for other Arctic coupled ocean-ice models (Stark et al., 2008; Johnson et al., 2012; Schweiger et al., 2012; Yang et al., 2014; Smith et al., 2015, Q. Wang et al. 2016) and even reanalyses (Uotila et al, 2018). Xie et al. (2016) have tested

assimilation of thin SIT (<0.4 m) from SMOS, and show that the assimilation slightly reduced the SIT overestimation near the sea ice edge. The recent availability of the weekly SIT from CS2SMOS provides an opportunity for the TOPAZ4 to constrain better the SIT error in the Arctic. This study aims at identifying a suitable practical implementation for assimilating C2SMOS data set and assess its usefulness for the Arctic reanalysis. Although it is expected that a better initialisation of SIT anomalies will enhance the predictability of the system, this is beyond the scope of this paper. A similar assessment over the same time frame has been carried out in the Arctic Cap Nowcast/Forecast System (ACNFS) by Allard et al. (2018) revealing significant improvements of bias and RMSD but little changes in ice velocity except in marginal seas. The proposed study in complementary to Allard et al. (2018) because the TOPAZ4 prediction system uses a more rudimentary sea ice thermodynamics (no explicit ice thickness distribution) but a more advanced ensemble-based data assimilation method (TOPAZ4 uses strongly coupled data assimilation of ocean and sea ice, meaning that sea ice observation will impact also the ocean and vice versa with a flow dependent assimilation method, see Penny et al., 2017; Kimmritz et al., 2018).

Section 2 describes the TOPAZ4 system: namely the coupled ocean and sea ice model, the implementation of the EnKF and the observations used for data assimilation and validation. In section 3, we carry an Observing System Experiment (OSE) comparing the two reanalyses: one using the standard observation types used in operational setting and another assimilating the CS2SMOS in addition. Then the performance of the two runs is presented against both assimilated and non-assimilated measurements. Section 4 presents the impacts of assimilating the CS2SMOS on sea ice drift and the integrated quantities for sea ice, and measures its relative impact compared to other assimilated observations. A summary is provided in the last Section.

2. TOPAZ4 system descriptions and observations

2.1 The coupled ocean and sea-ice model

TOPAZ4 is a forecasting ocean and sea-ice system developed for the Arctic, having been operational since the early 2000s (Bertino and Lisæter, 2008). It uses the Hybrid Coordinate Ocean Model (HYCOM: version 2.2) developed at

University of Miami, which has been successfully applied in global and regional oceans (Chassignet et al., 2003; Counillon and Bertino, 2009; Metzger et al 2014; Xie et al., 2018). The model grid is constructed using conformal mapping (Bentsen et al., 1999) with a 12-16 km resolution shown in Fig. 1 (left). The model uses 28 hybrid layers with reference potential densities selected specifically for the North Atlantic and the Arctic regions (Sakov et al. 2012). The model is forced by atmospheric forcing from ERA-Interim. A barotropic inflow of Pacific Water is imposed through the Bering Strait, which is balanced by an outgoing flow through the southern model boundary. It has an averaged transport of 0.8 Sv, and varies seasonally with a minimum (0.4 Sv) in January and a maximum (1.3 Sv) in June consistently with observations (Woodgate et al. 2005). The model accounts for river discharge, for which a seasonal climatology is estimated by feeding the run off from ERA-interim (Dee et al., 2011) into the Total Runoff Integrating Pathways model (TRIP, Oki and Sud, 1998) over the period 1989–2009.

A simple sea ice model using a one-thickness category has been coupled to HYCOM. The sea ice and the ocean are thus coupled every 3 hours and exchange momentum, salt and heat on the ocean model's Arakawa C-grid. The sea ice thermodynamics treat precipitations on ice as snow whenever surface air temperature is below zero (Drange and Simonsen, 1996). The ice dynamics uses the elastic-viscous-plastic rheology (Hunke and Dukowicz, 1997) with the modification suggested by Bouillon et al. (2013). There is a 0.1 m limit in the model for the minimum thickness of both new ice and melting ice.

2.2 Implementation of the EnKF in the TOPAZ4 system

The TOPAZ4 system uses a deterministic Ensemble Kalman Filter (DEnKF, Sakov and Oke, 2008), which solves the analysis without the need to perturb the observations and is therefore a square-root filter implementation of the EnKF. In the DEnKF, if the model state is represented by $\mathbf{x}$, the ensemble mean is updated by equation:

$$\bar{\mathbf{x}}^a = \bar{\mathbf{x}}^f + \mathbf{K}(\mathbf{y} - \mathbf{H}\bar{\mathbf{x}}^f), \tag{1}$$

where the superscripts "f" and "a" refer respectively to the forecast and the analysis. Following Xie et al. (2017), the model state vector $\mathbf{x}$ contains 3-

189 dimensional ocean variables in the native hybrid coordinates (u- and v-
190 components of the current velocities, temperature, salinity and model layer
191 thickness), the 2-dimentional ocean variables (u- and v-components of the
192 barotropic velocities, barotropic pressure, and mixed layer depth) and three sea
193 ice variables: ice concentration, ice thickness and snow depth. The assimilated
194 observations are represented by the vector **y** without perturbation, and the
195 observation operator **H** projects the model variables on the observation space.
196 The misfit between the model and the observation - the bracket term in Eq. (1),
197 is the innovation. The Kalman gain **K** is calculated by:

198 $$\mathbf{K} = \mathbf{P^f H^T [H P^f H^T + R]^{-1}}$$ (2).

199 Where **P^f** is the background error covariance matrix, **R** is the observation error
200 covariance matrix, and the superscript "T" denotes a matrix transpose. The
201 background error covariance is approximated from the ensemble anomalies **A**
202 (where $\mathbf{A} = \mathbf{X} - \bar{\mathbf{x}}I_N$, $I_N = [1, ... ,1]$, N being the ensemble size) as $\mathbf{P} = \frac{\mathbf{AA^T}}{N-1}$. Here,
203 **X** denotes the ensemble of model states. The observation errors are assumed
204 to be uncorrelated (i.e. the matrix **R** is diagonal). While this practical assumption
205 is not valid for interpolated observations, a diagonal approximation combined
206 with an inflation of the observation error can make a reasonable approximation
207 when the error spatial structure is unknown (Stonebridge 2018). A localization
208 is used in order to reduce the sampling error with a radius of 300 km and a
209 polynomial tapering function (in a local analysis framework).

210 The practical implementation of the model and its perturbations follow Sakov et
211 al. (2012): the model errors include joint perturbations of winds, heat fluxes as
212 originally recommended by Lisæter et al. (2007). The precipitation perturbation
213 has however been increased from 30% to 100%, following a log-normal
214 probability distribution of errors (Finck et al. 2013), which also increased the
215 spread of ice thickness.

216

217 ### 2.3 Observations for assimilation and validation

218 The following observations are assimilated sequentially every week in the
219 TOPAZ4 system (Xie et al. 2017): along-track Sea Level Anomaly; in situ
220 profiles of temperature and salinity; gridded Operational Sea Surface
221 Temperature and Sea Ice Analysis (OSTIA) SST; Ocean and Sea Ice Satellite

222 Application Facility (OSI-SAF) sea ice concentration and sea ice drift from
223 satellite observation (Lavergne et al., 2010). All measurements are retrieved
224 from CMEMS, http://marine.copernicus.eu, and are quality controlled and high-
225 resolution observations are "superobed": all observations falling within the
226 same grid cell are averaged and the observation uncertainty is reduced
227 accordingly (Sakov et al., 2012). For SST and ice concentration, we only retain
228 the observation on the last day of the assimilation cycle. Similarly, only the sea
229 ice drifts during the last 2 days of the assimilation cycle are assimilated.

230 The weekly SITs of CS2SMOS were retrieved from
231 http://data.meereisportal.de/maps/cs2smos/version3.0/n on the period from
232 March 2014 to March 2015. This product is gridded with a resolution of
233 approximately 25 km. The provider uses optimal interpolation to blend the
234 measurements of CryoSat-2 and SMOS based on their uncertainties and their
235 spatial covariance. An estimate of the observation error is provided with the
236 data set but only accounts for the errors related to the merging and interpolation
237 (Ricker et al., 2017). As such, we expect that this observation error is
238 underestimated since it misses both the sensor errors and the model-related
239 representation errors. In particular the mapping is based on a no-bias
240 assumption and error estimates do not account for inconsistencies between the
241 two satellites, like those reported by X. Wang et al. (2016) and Ricker et al.
242 (2017). With an EnKF assimilation system, underestimating the observation
243 error leads to an underestimation of the ensemble spread and makes the
244 system suboptimal, leading in the worst case to system divergence.
245 Underestimating the errors of one data type also lessens the impact of the other
246 assimilated observations since they compete for the control of a finite number
247 of degrees of freedom. This issue will be addressed in Section 4.3. On the other
248 hand, Oke and Sakov (2008) showed that the performance of the EnKF does
249 not degrade much when observation error is overestimated. It is therefore
250 necessary to increase the observation error to a level at least as high as the
251 optimal value for the performance of the filter (Desroziers et al., 2005; Karspeck,
252 2016).

253 In order to estimate the representation error for the SIT observation, we have
254 performed a preliminary sensitivity assimilation experiment for November 2014.
255 We used the diagnostics by Desroziers et al. (2005) as an indicative lower limit

for the observation error in the TOPAZ4 system based on the misfits to the CS2SMOS data. Desroziers et al. (2005) estimate the optimal observation error as the following matrix:

$$\tilde{\sigma}^o_{SIT} = \sqrt{\frac{1}{p}\sum_{j=1}^{p}(\mathbf{y}_j - \mathbf{H}\overline{\mathbf{x}}^a)(\mathbf{y}_j - \mathbf{H}\overline{\mathbf{x}}^f)} \tag{3}$$

where p is number of data assimilation steps in the sensitivity run (here 4), and $\mathbf{y}_j$ represents the observed SIT from CS2SMOS at the jth assimilation time. Here, the terms $\overline{\mathbf{x}}^a$ and $\overline{\mathbf{x}}^f$ represent the ensemble mean of the analysis and forecast states. In Fig. 2, the diagnosed observation errors from Desroziers et al. (2005) are larger than the mapping error included in CS2SMOS, but still do not account for biases in the CryoSAT2 and SMOS observations. The CS2SMOS mapping error is particularly low for sea ice below 0.5 m: about 4 times lower than the uncertainties obtained by error propagation in the SMOS processing chain (used in Xie et al. 2016), which would make the assimilation of SMOS SIT too strong. The Desroziers diagnosed errors gradually increase with ice thickness, although they vary unrealistically for SITs above 3 m, possibly due to low counts of either modelled or observed ice thickness in certain thickness ranges. In view of the above considerations, we have added a cautious correction term to the CS2SMOS mapping error estimate, which simply increases linearly with the observed SIT.

$$\varepsilon_{Offset} = \min(0.5, 0.1 + 0.15 * \mathbf{d}_{SIT}) \tag{4},$$

where $\mathbf{d}_{SIT}$ is the observed sea ice thickness. At low SIT, the resulting values are slightly higher than those used in Xie et al. (2016) and comparable to the Desroziers diagnostics. At SITs of 1.5 m, for which SMOS and CS2SMOS overlap, the added correction is comparable to reported differences between the two satellites: about 20 cm in the Beaufort Sea and 1 meter in the Barents Sea, see Table 3 in Ricker et al. (2017). Tilling et al., (2018) show that the standard deviations between the CryoSat-2 and independent measurements are between 30 and 70 cm depending of the source of observation and increase with ice thickness (their Figure 16). It should be noted however that the processing of CryoSat2 data differs in CPOM and AWI's algorithms. The total observation error including the added term is shown with blue-squared line in

Fig. 2. In the following, we will only use the corrected observation error for the CS2SMOS SIT.

3. Observing system experiment runs and validations

3.1 Experiment and independent observations for validation

A parallel OSE is conducted from 19th March 2014 until end of March 2015. The two assimilation runs cover two special time periods: the onset of ice melting in March-April 2014 following by a data period free of CS2SMOS, then a whole cold season from October 2014 to March 2015. The control run named the **Official run** uses the standard observational network in the TOPAZ4 system (Xie et al. 2017), which assimilates on a weekly cycle the SLA, SST, in situ profiles of temperature and salinity, SIC and sea ice drift (SID) data. Another assimilation run named the **Test run** includes as well the SIT from CS2SMOS. We discard the SIT closer than 30 km from the coast to account for differences of coastlines between the model and observations. The innovation of SIT in Eq. (1) is calculated in terms of sea ice volume:

$$\Delta\mathbf{SIT} = \mathbf{d}_{\text{SIT}} - \mathbf{H}\overline{(\mathbf{h} \times \mathbf{f})}_{\text{m}}, \qquad (5)$$

where $\mathbf{d}_{\text{SIT}}$ is the observed SIT from CS2SMOS as in Eq. (4), $\overline{(\mathbf{h} \times \mathbf{f})}_{\text{m}}$ is the ensemble mean of ice volumes forecasted by model. The f and h are SIC and ice thickness within the grid cell respectively. We assume the observation error is uncorrelated (**R** in Eq. (2) is diagonal). Although the minimal thickness in the model is set to 0.1 m, the ensemble mean from 100 model members can be as thin as 1 mm, so that we only reject the observed SIT if it is equal to 0. Every week, the SITs from CS2SMOS are considered to be at the analysis time, neglecting the time delay. The associated errors due to the sea ice motions or thermodynamic growth/melt of sea ice within one week remain small compared to the large SIT biases targeted in the present exercise.

In the following, we investigate the misfits of the forecasted model states by evaluating the bias and the root mean square difference (RMSD):

$$\text{Bias} = \frac{1}{L}\sum_{i=1}^{L}(\mathbf{H}_i\bar{\mathbf{x}}_i^f - \mathbf{y}_i) \qquad (6)$$

$$\text{RMSD} = \sqrt{\frac{1}{L}\sum_{i=1}^{L}(\mathbf{H}_i\bar{\mathbf{x}}_i^f - \mathbf{y}_i)^2} \qquad (7).$$

318 Where L is the total number of assimilation cycles during the study, $\bar{\mathbf{x}}_i^f$ is the

319 ensemble mean model state at the *i*th time, which is compared to the

320 observations $\mathbf{y}_i$.

321 Three types of independent SIT observations are used for validation. First, the

322 drifting Ice Mass Balance buoys (IMB: http://imb-crrel-

323 dartmouth.org/imb.crrel/buoysum.htm, Perovich and Richter-Menge, 2006).

324 Four IMB buoys are available during the experimental time period (2013F,

325 2014B, 2014C, and 2014F) and their trajectories are shown in Fig.1 (left).

326 Second, three upward looking sonar (ULS) buoys funded by the Beaufort Gyre

327 Exploration Project (BGEP, see http://www.whoi.edu/beaufortgyre) have been

328 moored in the Beaufort Sea. Their locations are shown with the red squares in

329 Fig. 1 (left). They estimate the sea ice drafts since October 2014. Third, the

330 NASA IceBridge Sea Ice Thickness Quick Look data

331 (https://nsidc.org/data/icebridge) collected in aerial campaigns estimate the SIT

332 in spring (Kurtz et al., 2013) with a better spatial coverage. The locations of the

333 quality-controlled SIT observations from IceBridge for March and April of 2014

334 and 2015, are shown with the yellow squares in Fig. 1 (left).

335

336 **3.2 Validation against CS2SMOS and innovation diagnostics**

337 The first assimilation time is the 19th March 2014 and the last is the 25th March

338 2015. The monthly SITs from the two OSE runs are compared to CS2SMOS in

339 Fig. 3. The SITs in April 2014 are presented for comparison in the upper panels

340 of Fig. 3. In the Official run, the thick sea ice to the north of the CAA is

341 underestimated but thickens slightly in the Test run: the 3 m SIT isoline covers

342 a wider area, in better agreement with the observations. The areas of thinner

343 sea ice north of the Barents Sea, west of the Kara Sea, and the coast of the

344 Beaufort Sea, which were too thick in the Official run, have all been improved

345 also shown by reduced area delimited by the isolines of 1 m or 2 m SIT in the

346 Test run.

347 After summer of 2014, measurements of SIT from CS2SMOS restart at the end

348 of October. Results are presented for November 2014 in Fig. 3: the thick sea

349 ice in the central Arctic has been further improved in the Test run. The thickest

350 sea ice (> 3 m) is located near the northern coast of Canada instead of north of

351 Greenland in the Official run. The averaged SIT in the Test run around the North

352 pole (>80°N), is increased from 1.3 m in the Official run to 1.6 m, which is closer

353 to CS2SMOS by 43%. In the marginal zones - East Siberian Sea, Laptev Sea,

354 and Kara Sea - the SITs in the Official run is too thin, but is thicker in the Test

355 run. Improvements in marginal seas are due to the contribution of SMOS, while

356 improvements in the ice pack are more likely due to CryoSat-2.

357 In the last month of the experimental period (March 2015), the thick sea ice

358 pattern in the Test run, shown as the 2 m isoline, is more similar to CS2SMOS.

359 The maximal SIT within the 4 m isoline is located north of the CAA in the Test

360 run and in CS2SMOS, while in the Official run it spreads further out from the

361 northern coast of Canada to north of Greenland. In addition, the SIT north of

362 the Fram Strait is thicker than in the Official run. The SIT is similarly improved

363 near the coast of the Beaufort Sea and to the northwest of Svalbard. As

364 expected with data assimilation, the Test run agrees clearly better with the

365 assimilated product. Those improvements are largest in the ice pack and in the

366 marginal Seas, where the model deviates considerably from the CS2SMOS

367 SITs. On the contrary, the thickness near the sea ice edge is not strongly

368 impacted by the assimilation.

369 The above results are confirmed quantitatively by comparing misfits of weekly

370 SIT from the two runs with the corresponding CS2SMOS observations. Time

371 series of bias and RMSD calculated as in Eq. (6-7) are shown in the top panel

372 of Fig. 4. In the beginning of the period, the SIT RMSD in the Test run decreases

373 quickly from 0.6 m to 0.4 m before the observations are interrupted for the

374 summer. The biases are reduced equally in both runs. After the observations

375 resume in the end of October 2014, the SIT RMSD is comparable between the

376 two runs but the bias is slightly lower in the Test run. There is large spike in the

377 bias and RMSD for both systems that relates to an inaccuracy of the CS2SMOS

378 observations (see Section 4.2). After the spike, the RMSD and bias in the Test

379 run are lower than in the Official run. The bias in the Test run converges to 0

380 and fluctuates around that level but this is probably not due to the assimilation

381 since the bias in the Official run also converges to 0 during that time. This is

382 rather due to the compensation of seasonal and regional errors. On average,

383 the SIT bias (too thin) is decreased from 15 cm to 5 cm by the assimilation of

384 CS2SMOS. The RMSD of SIT is 38 cm in the Test run, which corresponds to a

385 reduction of 28.3% relative to the error in the Official run.

386 The innovation statistics taken at each assimilation time are used to evaluate

387 how well our data assimilation system is calibrated. In the reliability budget of

388 Rodwell et al. (2016), the total uncertainty of an ensemble data assimilation

389 system is calculated as follows:

$$\sigma_{diag} = \sqrt{Bias^2 + \sigma_{en}^2 + \sigma_o^2} \quad , \tag{8}.$$

390

391 where the *Bias* term – i.e. the mean innovation (shown as blue-circled lines) -

392 is calculated as in Eq. (6) at a given assimilation time step, while σ_{en} and

393 σ_o represent respectively the ensemble spread and the standard deviation of

394 the observation errors at the same assimilation time. If the data assimilation

395 system is reliable, the diagnosed total uncertainty should be close to the RMSD,

396 formulated in Eq. (7). Fig. 4 shows that the pink and red lines are evolving

397 reasonably in phase but that the diagnosed error σ_{diag} is twice larger than the

398 RMSD, meaning that our system is overdispersive. The error budget shows that

399 the observation error (σ_o) itself is too large, suggesting that the offset term in

400 Eq. (4) is overestimated, which we do not expect as a serious problem as

401 explained above.

402 The innovation statistics for SIC are mostly identical in the two runs (not shown),

403 the mean misfits for SIC vary around ±4% and are most of the time lower than

404 12%, which is consistent with the evaluation of the TOPAZ4 reanalysis in Xie

405 et al. (2017). It is somewhat disappointing that improvements of ice thickness

406 do not yield visible benefit to ice concentration, but on the other hand a

407 degradation could also have been possible in case the thermodynamical model

408 had been over-tuned to an incorrectly simulated thickness. It should also be

409 noted that the innovations statistics of SST and SLA are also indiscernible in

410 the two runs and not shown either.

411

412 **3.3 Validation against independent SIT observations**

413 *3.3.1 Ice Mass Balance Buoys*

414 Four IMB buoys are available as independent validation of the impact of the

415 assimilation of CS2SMOS. The buoys are drifting in the Canadian Basin (Fig.

416 1), and only one buoy (2013F) lasted during the whole experimental time period

417   shown (upper panel of Fig. 5). This buoy exhibits the seasonal variability of SIT:

418   it reaches 1.5 m in spring 2014, decreases down to 1.0 m in September and

419   rises again to 2 m in March 2015. The seasonal SIT cycle of the Official run

420   shows excessive seasonal variability, with a thin bias in summer 2014 and a

421   thick bias during the two winters. In the Test run (shown as the red-dashed line)

422   the seasonal cycle is dampened and more consistent with the observations.

423   The bias is still quite large around March-April and remains so even at the end

424   of the study period. It should be noted that the impact of CS2SMOS seems

425   largest in summer, when no observations are assimilated. This illustrates the

426   persistent effects of winter SIT improving the predictability of the summer Arctic

427   sea ice as shown in Mathiot et al. (2012). When CS2SMOS is assimilated again

428   in the fall 2014, the Test run initially overestimates slightly the SIT measured at

429   the buoy compared to the Official run but is slowly improving as the data is

430   assimilated. The time-averaged SIT RMSD for buoy 2013F is reduced from

431   0.33 m in the Official run down to 0.25 m in the Test run, a reduction by 24.2%.

432   Two other buoys (2014B and 2014C) cover the early months of the

433   experimental period. The two runs are initially biased with a too thick SIT by 0.5

434   m and 0.2 m compared to 2014B and 2014C. At buoy 2014B, there is a slight

435   error reduction during the assimilation period that continues beyond the

436   assimilation window, similarly to buoy 2013F. At buoy 2014C however, although

437   the error is reduced during the analysis period, the two assimilation runs

438   converge during the summer. At these three buoys the assimilation corrects the

439   mean SIT values and the amplitude of the seasonal cycle but has little influence

440   on the phase of the seasonal cycle.

441   The buoy 2014F covers the last 6 months of the experimental period. At that

442   buoy, the assimilation seems increase the errors. It should be noted however

443   that the constant SIT at buoy 2014F seems unlikely or not representative of the

444   area.

445   *3.3.2 The BGEP mooring buoys*

446   In order to convert the sea ice draft measured by ULS from the BGEP buoys to

447   SIT, we used the balance equation as in Tilling et al. (2018):

448    $$\mathbf{d}_{SIT} = \frac{d_i \rho_w - h_s \rho_s}{\rho_i} \tag{9}$$

449 where $\mathbf{d}_{SIT}$ is the sea ice thickness, d_i is sea ice draft, h_s is snow depth, ρ_i is sea

450 ice density, ρ_s is snow density and ρ_w is seawater density. The above densities

451 are set to 900, 300, and 1000 kg/m^3 as in the TOPAZ model. d_i is the sea ice

452 draft measured by ULS at the fixed locations (see Fig. 1). The snow depth is

453 taken from the model daily snow depths, averaging the two model runs and

454 interpolating at the buoys locations.

455 The SIT time series of the measurement and of the two runs are shown on Fig.

456 6, from October 2014 onwards. The gray error bars depict the daily standard

457 deviation. The data indicates an increasing SIT from around 0.5 m in October

458 2014 to nearly 2 m in March 2015. The observed SIT at mooring 14D shows a

459 very large daily variability from end of October to November 2014, especially

460 compared with that of moorings 14A and 14B.

461 The weekly SITs from CS2SMOS match well the data with RMSDs of 15, 19

462 and 39 cm during the 6 months, which is lower than in the two model runs. Still,

463 the SIT from CS2SMOS overestimates SIT from October 2014 to middle

464 January 2015 compared to the mooring 14B, and between in Oct and Nov of

465 2014 for mooring 14A. The SITs in the Official run are overestimated in all three

466 locations. The SIT RMSDs are 41, 23 and 51 cm respectively compared to SIT

467 measurement from the three moorings. The SITs in the Test run are closer to

468 observations, thanks to the data assimilation of the SIT from CS2SMOS. The

469 SIT RMSDs in the Test run are respective 25, 33 and 36 cm for moorings 14A,

470 B, D. The error is reduced for moorings 14A and 14D compared to the Official

471 run but increases for mooring 14B, mostly due to the initial mismatch between

472 CS2SMOS and the mooring. Similarly to the comparison with IMB buoys,

473 moorings suggests that error of SIT in the Beaufort Sea is reduced by

474 assimilation of CS2SMOS.

475

476   *3.3.3 IceBridge Quick Look*

477 Another independent observation of SIT with better spatial coverage is the SIT

478 Quick Look data from airborne instruments during NASA's Operation IceBridge

479 campaign (Kurtz et al., 2013). Those are available via the National Snow and

480 Ice Data Center (NSIDC), albeit for the months of March and April only. Note

481 that the airborne SITs have been reported to be slightly low-biased by about 5

cm compared to in situ measurements (King et al., 2015). Figure 7 shows all observed SITs (upper-left panel) from IceBridge, collected during March and April of 2014-2015. All observed SITs are located in the Canadian Basin and north of Greenland and cover most of the area where sea ice is thicker than 3 m. Thicknesses between 1~3 m are measured in the Beaufort Sea. The two simulated SITs in the two model runs show systematic differences of SIT (see upper-right panel of Fig. 7): the Test run SIT has been thinned in the Beaufort Sea and thickened near the North Pole. On average, the SIT in the Test run is increased by 0.1 m and by 0.27 m north of 80°N. Fig. 10b shows that the frequency distributions of SITs at the International Arctic Buoy Program (IABP) buoys (locations shown to the right of Fig. 1) have been significantly adjusted between the two runs: The thick sea ice (>2.2 m) becomes more abundant in the Test run and the relatively thin sea ice (0.5-1.7 m) more abundant in the Official run. The averaged SIT thus increases from 1.52 m to 1.62 m in the Test run.

The comparisons of the two OSE runs to the IceBridge data are presented in the bottom panels. The sea ice in the Official run is too thin at the north of the CAA and north of Greenland, with a deviation larger than 1.5 m. In the Beaufort Sea on the contrary, the model is too thick by 0.5 to 1 m. This bias is consistent with that reported in Xie et al. (2017), where the TOPAZ4 reanalysis (Official run) was compared to ICESat observations in the period 2003-2008. In the Test run, the biases are slightly reduced by SIT assimilation, mainly in the Beaufort Sea and north of Greenland, but the reduction is smaller than the remaining error. On average, the SIT RMSD is 1.05 m, which corresponds to a reduction of 12.5% compared to that in the Official run.

The regression of the SIT observations from IceBridge to the two OSE runs is shown in Fig. 8. The Test run shows improved linear correlations to the observation. The offset at the origin is reduced (0.52 m instead of 0.93 m) and the slope is closer to 1 than in the Official run. The linear correlation in the Test run is slightly increased as indicated with the square correlation R^2. There is still a lot of spread which keeps the correlation is on the low side. However, the model still underestimates the thickest ice observed in IceBridge, with a bias as high as 2 m.

4. Impact of CS2SMOS in the data assimilation system

The above results and assimilation diagnostics confirm that the SIT misfits can be controlled - to some degree - by assimilation of the CS2SMOS data, without visible degradation of other assimilated variables. To better understand the advantages and the limits of assimilating the merged SIT product, we further evaluate the impact of CS2SMOS in the assimilation system: first the repercussions on other sea ice variables and integrated quantities, and then through a quantitative impact analysis of CS2SMOS relatively to other assimilated observation types.

4.1. Impact on the sea ice drift

The EnKF implemented in TOPAZ4 updates all the variables in the model state vector using flow-dependent multivariate covariances from the ensemble members (Eqs. 1 and 2). The direct assimilation update of ice drift is however short-lived: the ice drift vectors quickly readjust to wind forcing after assimilation, so the ice drift changes are mostly caused by dynamical readjustments, related to the updated ice thickness and ice concentrations. By the first order approximation of the two-dimentional momentum equation (e.g., Hibler 1986; Hunke and Dukowicz, 1997), the drift velocity of sea ice is mainly controlled by 1) the interactions of atmosphere-sea ice, 2) the interactions of ocean-sea ice and 3) the internal sea ice forces which can be represented by the stress tensor σ_i. The work of Olason and Notz (2014, thereafter called ON14) shows from observations that ice thickness is the main driver changes of ice drift in winter (December to March), while the concentration is the main driver in summer (June to November) and ice drift may increase independently from concentration of thickness in transition periods due to increasing fracturing.

Following the EVP rheology in Hibler (1979), the stress tensor σ_i is forced by a pressure term Q which takes a function of the sea ice thickness and concentration only.

$$Q = P^* d_{SIT} \exp(-C_0(1 - A_{SIC})), \qquad (10)$$

Where C_0 and P^* are empirical constants, $\mathbf{d}_{SIT}$ is SIT, and A_{SIC} is sea ice concentration. ON14 thus show that this type of rheology is able to reproduce the changes of ice drift whenever they are related to changes of concentration and thickness, although not the changes during the transition periods. The

549   sensitivity of ice drift to ice thickness can be directly adjusted by tuning the value

550   of P* in Eq. (10) (see for example Docquier et al., 2017). In the TOPAZ4 model,

551   the sea ice dynamics assume a viscous-plastic material with an adjustment

552   mechanism at short timescales by elastic waves (called EVP, Hunke and

553   Dukowicz, 1997). The ice thickness does as well have an influence on the ice

554   concentrations in the summer due to melting, but this influence is limited in

555   TOPAZ4 by the assimilation of ice concentrations. The winter months in the

556   seasonal cycle (see Figure 6 in ON14) indicate that a 10% increase of ice

557   thickness can reduce the ice drift by 9%. Areas of thinner ice are much more

558   sensitive (see Figure 5 in ON14) and therefore the above numbers are subject

559   to possible biases of ice thickness. The sensitivity on seasonal time scales may

560   also differ from the sensitivity on a weekly time scale (that of the TOPAZ4

561   assimilation cycle).

562   The evaluation in Xie et al. (2017) shows the model drift of sea ice is

563   overestimated by 2 km d^{-1} on average on the Arctic with an uncertainty of 5 km

564   d^{-1}. The thickness of thick ice is also too thin, consistently with the too fast drift

565   (Figures 14 and 17 in Xie et al., 2017). So, the assimilation of ice thickness is

566   expected to improve the ice drift by dynamical model adjustment. Figure 9

567   shows monthly differences of the 2-day sea ice drift (SID) compared to the OSI-

568   SAF estimates based on passive microwave data in April 2014, December 2014

569   and February 2015. The SID in the Official run is too fast in the central Arctic

570   where the SIT was found too thin in Fig. 3. Despite of the relatively small

571   assimilation impact of CS2SMOS on the SID, there are improvements across

572   the Arctic in all winter months.

573   The RMSD of sea ice drift speed in two-days trajectories is reduced by about

574   0.1-0.2 km in April 2014 and February 2015 for the whole Arctic, which

575   corresponds to a reduction of less than 5% of the RMSD. However, near the

576   North Pole (north of 80°N), the reduction of drift RMSDs is more important, by

577   about 0.4-0.5 km. In December 2014 and February 2015 it is about 8-9% of the

578   error in the Official run. Near the North Pole the averaged SIT in March 2015

579   (Fig. 3) is about 10% thicker in the Test run than in the Official run. The impact

580   is more important there than in the rest of the Arctic and well in line with the

581   sensitivity found in ON14. Additionally, there is a small reduction of the fast SID

582   bias but in the case of TOPAZ4, such biases are dependent on the tuning of

583   the drag coefficients between sea ice and the air or the ocean, which has been
584   optimized for the SIT distribution of the TOPAZ free run. The tuning of the drag
585   coefficient adopted by Rampal et al. (2016) is independent from SIT values
586   since it only uses free-drifting ice for tuning.

587   To evaluate the potential impact of assimilating the SIT from CS2SMOS on the
588   sea ice motion, we further utilize the data set from the IABP buoys which began
589   in 1990s to monitor ice motion throughout the Arctic Ocean. Only trajectories
590   longer than 30 days and reporting more than 5 times per day are used to
591   estimate the daily drift speed of sea ice. To avoid buoys in open water, the
592   observations are selected based on sea ice concentration (>0.15) and ice
593   thickness (>5 cm) at the nearest model grid cell in both runs. Furthermore, the
594   dataset is restricted in the central Arctic, (delimited by a red line in Fig. 1), where
595   water is deeper than 30 m and further away from the coast than 50 km. A total
596   of 151 buoys are left from this selection, which provide 21,793 daily estimates
597   of drift speed.

598   The speed distribution for daily drift of sea ice from IABP is shown by a
599   histogram in Fig. 10a. In the central Arctic, the averaged drift speed is about
600   10.6 km d^{-1} (consistently with Allard et al., 2018) and most speeds (95%) are
601   slower than 24 km d^{-1}. The difference of drift distributions between the two runs
602   is minor compared to the difference to the IABP data. Restricting the analysis
603   to the area North of 80 degrees, the two runs show larger differences in SIT
604   with a Test run about 30 cm thicker (Fig. 10d), the resulting difference in SID in
605   that area is small (0.2 km d^{-1}) and tends to degrade slightly the performance by
606   slowing down the drift speed (Fig. 10c). This is somewhat contradictory to the
607   analysis with OSI-SAF data which indicated a too fast model drift and smaller
608   errors in the Test run. This inconsistency may be due to the poor spatial
609   coverage of the IABP buoys. In Fig. 1 we can see that buoys north of 80°N are
610   mainly found in the Eurasian Basin and sample poorly the region between the
611   Transpolar Drift Stream and the Beaufort Gyre (Sumata et al., 2014), where the
612   SID misfits are largest and where the model drift is too fast. This poor coverage
613   of IABP buoys may as well explain why the SID comparisons in Allard et al.
614   (2018) were inconclusive.

615

616   **4.2 Impact on the sea ice extent and volume in the central Arctic**

617 In Fig. 3, we show that the Arctic SIT has been improved everywhere, the
618 assessment of the sea ice drift is less conclusive but tends to suggest a slight
619 improvement localized in the central Arctic. However, improving the quantitative
620 match with available observations does necessarily warrant the physical
621 consistency of basin-scale integrated quantities. The impact of CS2SMOS on
622 the Arctic-wide sea ice extent (SIE) and the sea ice volume (SIV) are
623 investigated for the two runs and compared with the estimates from CS2SMOS
624 and OSI-SAF respectively. Due to differences of resolution and land mask
625 (especially important in the Canadian Archipelago), we focus on the central
626 Arctic domain shown as the red line in the right panel of Fig. 1, excluding parts
627 of the marginal seas.

628 Figure 11 shows the time evolutions of SIE and SIV in the two Official and Test
629 runs. Both are calculated by daily averages in the two model runs. The SIE is
630 classically calculated in the area where the SIC is not less than 15% in the
631 Central Arctic. The SIE shows the expected seasonal cycle with the minimum
632 (close to 3×10^6 km^2) in September 2014 and saturates at a maximum value
633 corresponding to the area of the Central Arctic region (around 6×10^6 km^2) from
634 January to March. The timing of the minimum and maximum from the two model
635 runs agree very well with the observed in OSI-SAF and CS2SMOS (using the
636 weekly concentration from the CS2SMOS product). We can also notice the
637 impact of the weekly assimilation cycle that causes some "sawtooth"
638 discontinuity and indicates that the model tends to both melt too fast in August
639 and freeze too fast in September-October. Overall the SIE differences between
640 the two runs (about 8,000 km^2) are indiscernible during the experimental time
641 period.

642 The time evolutions of the SIV in the two runs show larger differences in the
643 lower panel of Fig. 11. The maximum in the Test run is close to 12×10^3 km^3 in
644 April-May of 2014 and again end of March 2015, and the minimum is close to
645 5×10^3 km^3 in September 2014. On average, the SIV difference in the two OSE
646 runs is about 1,000 km^3, with lower volume in the Official run. Assimilation of
647 the CS2SMOS data yields an annual increase of the SIV by about 8% relative
648 to that in the Official run. The signature of the assimilation cycle is generally
649 less pronounced than on SIE, except in August 2014 due to the SIC updates
650 that are positively correlated to SIT in the summer (as noted in Lisæter et al.,

651 2003). Compared to the observed SIV from the weekly CS2SMOS, the
652 underestimation is significant at beginning of the runs (about 3×10^3 km^3), but
653 corrected by one third through the first month of assimilation of CS2SMOS.
654 When the CS2SMOS data are missing, the gap between the two runs remains
655 constant throughout the summer due to the long memory of winter ice, as
656 previously noted with the assimilation work of ICESat SIT data in Mathiot et al.
657 (2012). After the end of the summer during which no data of CS2SMOS are
658 available,the SIV from the Test run is in better agreement with the first
659 observed SIV from CS2SMOS. This indicates that the TOPAZ4 Official run has
660 underestimated SIV due to the history of the reanalysis but not as a systematic
661 tendency towards a bias state. The SIV estimates from observations
662 occasionally present sudden discontinuities that seem unrealistic for a large
663 integrated quantity such as the SIV of the central Arctic area. These
664 discontinuities are larger than what the data assimilation system would expect
665 based on the assumed observation error statistics given above. But the time
666 series indicate that the EnKF does, as the name indicates, filter out part of the
667 discontinuities so that only the major spike in early November 2014 causes a
668 discontinuity in the Test run. Fig. 12 shows that the spike corresponds to a large
669 homogeneous increase of SIT in all marginal seas between 26th Oct and 2nd
670 Nov 2014, followed by a large decrease in the subsequent week. The weekly
671 SIT innovation on the 2nd Nov reveals that the increase is largest south of the
672 Eurasian Basin and around the Fram Strait. There, the SIT is thinner than 0.3
673 m on the 26th Oct which may suggest that the problem comes from the SIT
674 measurement from SMOS. Until such inconsistencies are resolved in the
675 dataset, we would recommend to either discard the first weeks of observations
676 or increase the observation error during that period.

677

678 **4.3 Quantitative impact for the observational network**

679 The value of the Degrees of Freedom for Signal (DFS) is commonly used to
680 monitor the relative impact of different observations in a data assimilation
681 system (ref. Cardinali et al, 2004; Rodgers 2000; Xie et al, 2018), and is
682 calculated as follows:

683
$$\text{DFS} = tr\left(\frac{\partial \hat{y}}{\partial \mathbf{y}}\right) = tr\left\{\frac{\partial [\mathbf{H}(\bar{\mathbf{x}}^a)]}{\partial \mathbf{y}}\right\} = tr(\mathbf{KH}) \qquad (11).$$

684   Where $\hat{y}$ is the analyzed observation vector, the observation operator **H** is same

685   in Eq. (1), and the term *tr* is the trace operator. The DFS is easily calculated

686   and stored while performing the analysis with ensemble data assimilation (see

687   Sakov et al. (2012) for an application to the TOPAZ4 system with the EnKF). It

688   measures the reduction of uncertainty caused by a given observation type

689   expressed as a number of equivalent degrees of freedom. Note that the DFS

690   depend on the observation error statistics but not on the actual observation

691   values (see equation 11). A DFS of 0 indicates that the observation has no

692   impact at all, and a DFS equals to the total number of degrees of freedom

693   indicates that the observation has so much impact that it has collapsed the

694   ensemble to a single value. As the analysis is solved either in observational

695   space or in ensemble space (depending on which is computationally cheapest),

696   the DFS cannot exceed the smaller of the ensemble size and the number of

697   observations used for the local assimilation. The DFS quantity is linear and can

698   be split by observation types and accumulated in time periods. The averaged

699   DFS for the *k*th type of observation can then be noted by $\overline{DFS_k}$, and thus a

700   corresponding Impact Factor (IF) is defined as:

701
$$IF_k = \frac{\overline{DFS_k}}{\sum_{i=1}^{O} \overline{DFS_i}} \times 100\% \tag{12}.$$

702   Where *o* represents the number of different observation types assimilated in

703   this time period. IF_k represents the relative impact of the kth type of observations

704   with respect to the whole observation network.

705   Figures 13 and 14 show the IF_k for different observations assimilated in the Test

706   run averaged in two typical months: in November 2014 and in March 2015. The

707   SIC impacts are dominant close to the sea ice edge and in the CAA region in

708   the November, with an average IF of 22.7% in the whole Arctic. The SIT impact

709   from CS2SMOS is largest in the central Arctic in November 2014. A relatively

710   smaller impact (>20%) is also noticeable in north of the Barents Sea and west

711   of the Kara Sea. In the open ocean, the SST and SLA have the largest impact.

712   Temperature and salinity profiles have locally an important effect in the ice-

713   covered Arctic, where a few of ice-tethered profilers (ITP) are available and the

714   uncertainty is large. Xie et al. (2016) applied the same DFS method to evaluate

715   the impact of thin SIT from SMOS only. The present results reveal, as expected,

716   much larger impacts of CS2SMOS SITs in the central Arctic, with only a few

717   isolated dips where the ITP profiles are available. The IF is higher where the

718   ice is thicker, even though the observation error increases as a function of ice

719   thickness. It indicates that the ensemble background errors increase even more

720   than the observation errors in thick ice by temporal accumulation of model

721   errors. For example, errors in precipitation grow as the snow accumulates in

722   the Fall, and the resulting inter-member variability of snow cover causes inter-

723   member variability of SIT due to the thermal isolation effect of snow.

724   In March 2015, CS2SMOS has again a large impact in the central Arctic relative

725   to other assimilated observations even though previous literature indicates a

726   lower impact in the midst of winter than when the ice is growing (Mathiot et al.,

727   2012). The relative IF of SIT indeed remains high even though the absolute

728   DFS is decreasing, due to the lower impact of other assimilated observations,

729   in particular SIC (Lisæter et al., 2003). On average, the IF value of CS2SMOS

730   is about 40%. The high values (>40%) are clearly separated into two areas: one

731   is to the north of the CAA and Greenland; another following the inner side of

732   the sea-ice edge in marginal ice zones. The former is primarily a CryoSat-2

733   contribution, while the latter corresponds to the thin SITs from SMOS. The high

734   IF in the polar hole is probably undesirable since the observations there are

735   merely extrapolated, so in the future applications we would recommend

736   discarding these data, in order to leave the polar hole filled instead with sea ice

737   advected from areas where trustworthy SIT observations have been

738   assimilated.

739

740   5. Conclusions and discussions

741   CS2SMOS is the first product to monitor the complete pan-Arctic SIT in a

742   systematic way, although only for the winter months. It is a combination of two

743   very different, yet very advanced, technologies onboard the SMOS and

744   CryoSat-2 satellites, calibrated against very few in-situ observations of SIT,

745   freeboard and snow depths. Altogether, the issue of measurements

746   uncertainties is particularly delicate for the assimilation of CS2SMOS data. On

747   the other hand, defining proper model background errors for SIT is just as

748   delicate, when considering that the simulated SIT accumulates errors both in

749   the sea ice dynamics (in particular the rheological model) and in the

750   thermodynamics. The Bayesian approach to confront these two uncertainties is

by Monte Carlo propagation of uncertainties, which is what is practiced in the present study for the model background error, although not for the observation error.

This study assesses the impact of assimilating the new SIT product from 19th March 2014 to 31st March 2015. Compared to the assimilated SIT CS2SMOS, the thin bias is reduced from 15 cm to 5 cm, and the RMSD also decreased from 58 cm to 38 cm, a reduction by 28.3%. Other innovation diagnostics show no degradation towards other assimilated variables –namely SIC, SSH, SST and TS profiles.

The SIT is also improved when compared to four independent drifting IMB buoys and three BGEP mooring buoys. The benefits persist throughout the summer although no SIT observations are available then, consistently with the experiments from Mathiot et al. (2012). This is important because it suggests that the model is not attracted to his bias solution. The assimilation reduces the low SIT biases north of the CAA and north of Greenland and the high bias in the Beaufort Sea compared to independent observations from Operation IceBridge. Both the thick pack ice in central Arctic and the thin ice in marginal seas are corrected. On average, the SIT errors in March- April of 2014 and 2015 are reduced by 15 cm, a reduction by 12.5% compared to the Official run. The dynamical adjustment following the assimilation of SIT has partially improved the sea ice drift speeds in the Test run where the SIT has thickened: the monthly averaged drift speed errors north of 80°N are reduced by 0.4-0.5 km per two days in December 2014 and February 2015 (8-9% reduction of the error). This has been revealed by satellite products but not IABP in situ buoys for which the spatial coverage is very poor. However, it should also be reminded that the drag coefficient used in the Test run were tuned for the Official run which has a biased SIT. One would expect some improvement with a retuned drag coefficient value. At term, we consider doing an online parameter estimation of key parameter such as the drag coefficient as tested in Massonnet et al. (2014).

In this study, the DFS information in the ensemble data assimilation system has been applied to quantitatively evaluate the relative contributions of all assimilated observation types. CS2SMOS has the highest impact near the northern coast of Canada, north of Greenland, and on the inner side of the sea

785 ice edge, where the contributions from CryoSat-2 and SMOS SIT were
786 expected. The results, compared to assimilating SMOS only in Xie et al. (2016),
787 show the importance of CryoSat-2, particularly in the winter months to constrain
788 the SIT offsets (also shown by Mu et al. 2018, in a coupled MITgcm model
789 system) and motivate the assimilation of CS2SMOS in the following reanalysis
790 of TOPAZ4. However, the impact of SIT observations may vary with the
791 evaluation of the modelling and observing system. Firstly, the SIC may have
792 been underestimated in central Arctic due to the simplicity of the present sea
793 ice model. Further planned developments of TOPAZ include a new model
794 rheology that is able to resolve the scaling laws of deformation of sea ice
795 (Rampal et al., 2016) and should therefore improve the background errors of
796 ice concentration in winter months and sea ice drift, increase the impact of SIC
797 and SID within the ice pack and reduce the estimated SIT impact accordingly.
798 Other planned changes such as the simulation of melt ponds are not expected
799 to influence these results directly since there are no melt ponds when the SIT
800 data is available. Lastly, if a large number of in situ profiles were available below
801 the sea ice, they would also compete with the SIT observations.
802 The above OSE results, like others, are necessarily contingent on adequate
803 specifications of observation errors. Those are very much simplified in the case
804 of CS2SMOS, which is not an uncommon case for remote sensing observations:
805 due to the complexity of the physics involved, the specified observation errors
806 are reflecting interpolation errors rather than a nonlinear propagation of errors
807 from their sources (Ricker et al., 2017). In the present study, an offset has been
808 added to account for this difference in Eq. (4), which results in a conservative
809 error estimate with respect to the classical Desroziers optimality criterion and a
810 suboptimal performance in the reliability budget analysis. In the one hand,
811 reducing the observation would have accelerate the convergence to observed
812 SIT and converge to a more accurate solution. On the other hand, this would
813 have made the EnKF less robust to the sudden inconsistencies in the
814 observations as seen in Fig. 11. Further versions of the CS2SMOS data will
815 hopefully improve their temporal continuity and the impact of the data can be
816 increased accordingly.
817 An alternative to using the scheme CS2SMOS data would have been to
818 assimilate the two data sets CryoSat-2 and SMOS SIT separately and let the

EnKF merge them together rather than relying on optimal interpolation, as successfully demonstrated by Mu et al (2018). This would for instance avoid assimilating observations in places where they are the pure result of interpolation/extrapolation but would not resolve the offset between the two satellites, which is arguably the most worrying issue as of the present state of the SMOS and CryoSat-2 data. The assimilation of the separate datasets will be attempted in the future when their consistency is further improved.

The current TOPAZ reanalysis is currently reaching 2016 and extended by one year every year. The current study clearly shows the added value of assimilating SIT. In 2020, a new TOPAZ reanalysis will be provided with the upgraded version of TOPAZ5 which will include SIT assimilation from 2010 onwards.

Acknowledgements

Thanks to the three anonymous reviewers for constructive comments. Thanks to Dr. J. A. Johannessen for discussions and to Dr. S. Hendricks and Dr. R. Ricker for sharing the CS2SMOS data on meereisportal.de. The authors acknowledge the support of CMEMS for the Arctic MFC. Grants of computing time (nn2993k and nn9481k) and storage (ns2993k) from the Norwegian Sigma2 infrastructures are also gratefully acknowledged.

Reference:

Allard, R. A., Farrell, S. L., Hebert, D. A., Johnston, W. F., Li, L., Kurtz, N. T., Phelps, M.W., Posey, P.G., Tilling, R., Ridout, A. Wallcraft, A. J.: Utilizing CryoSat-2 sea ice thickness to initialize a coupled ice-ocean modeling system. *Advances in Space Research*, 62/6), 1265-1280, http://doi.org/10.1016/j.asr.2017.12.030, 2018.

Bathiany, S., Notz, D., Mauritsen, T., Raedel, G., and Brovkin, V.: On the potential for abrupt Arctic winter sea ice loss. *J. Climate*, **29**, 2703–2719, https://doi.org/10.1175/JCLI-D-15-0466.1, 2016.

Bertino, L., and Lisæter, K. A.: The TOPAZ monitoring and prediction system for the Atlantic and Arctic Oceans, Journal of Operational Oceanography, 1(2), 15–19, doi: 10.1080/1755876X.2008.11020098, 2008

851   Bentsen, M., Evensen, G., Drange, H., and Jenkins, A. D.: Coordinate transformation on a
852   sphere using conformal mapping, Mon. Weather Rev., 127, 2733-2740,
853   doi:http://dx.doi.org/10.1175/1520-0493(1999)127<2733:CTOASU>2.0.CO:2, 1999.

854   Bouillon, S., Fichefet, T., Legat, V., and Madec, G.: The elastic-viscous-plastic method revised.
855   Ocean Modell., 7, 2-12, doi:10.1016/j.ocemod.2013.05.013, 2013.

856   Budikova, D.: Role of Arctic sea ice in global atmospheric circulation: A review. Global and
857   Planetary Change, 68,149-163, doi:10.1016/j.gloplacha.2009.04.001, 2009.

858   Cardinali, C., Pezzulli, S., and Andersson, E.: Influence-matrix diagnostic of a data assimilation
859   system, Q. J. R. Meteorol. Soc., 130, 2767-2786, doi:10.1256/qj.03.205, 2004.

860   Chassignet, E. P., Smith, L. T., and Halliwell, G. R.: North Atlantic Simulations with the Hybrid
861   Coordinate Ocean Model (HYCOM): Impact of the vertical coordinate choice, reference
862   pressure, and thermobaricity, J. Phys. Oceanogr., 33, 2504-2526. Doi:
863   http://dx.doi.org/10.1175/1520-0485(2003)033<2504:NASWTH>2.0.CO:2, 2003.

864   Comiso, J. C., Parkinson, C. L., Gersten, R., and Stock, L.: Accelerated decline in the Arctic
865   sea ice cover. *Geophys. Res. Lett.*, **35**, L01703, doi:https://doi.org/10.1029/2007GL031972,
866   2008.

867   Counillon, F. and Bertino, L.: High-resolution ensemble forecasting for the Gulf of Mexico
868   eddies and fronts, Ocean Dynam., 59, 83–95, doi:10.1007/s10236-008-0167-0, 2009.

869   Day, J. J., Hawkins, E., and Tietsche S.: Will Arctic sea ice thickness initialization improve
870   seasonal forecast skill?, Geophys. Res. Lett., 41, 7566–7575, doi:10.1002/2014GL061694,
871   2014.

872   Dee, D. P., Uppala, S. M., Simmons, A. J., Berrisford, P., et al.: The ERA-Interim reanalysis:
873   configuration and performance of the data assimilation system, Quart. J. Roy. Meteor. Soc.,
874   137, 553-597, doi:10.1002/qj.828, 2011

875   Desroziers, G., Berre, L., and Poli, P.: Diagnosis of observation, background and analysis-error
876   statistics in observation space. Q. J. R. Meteorol. Soc., 131(613), 3385-3396,
877   https://doi.org/10.1256/qj.05.108, 2005.

878   Docquier, D., François Massonnet, F., Barthélemy, A., Tandon, N. F., Olivier Lecomte, O., and
879   Fichefet, T.: Relationships between Arctic sea ice drift and strength modelled by NEMO-
880   LIM3.6. The Cryosphere, 11, 2829-2846, https://doi.org/10.5194/tc-11-2829-2017, 2017

881   Drange, H., and Simonsen, K.: Formulation of air-sea fluxes in the ESOP2 version of MICOM,
882   Technical Report No. 125 of Nansen Environmental and Remote Sensing Center, 1996.

883   Ferreira, A. S. A., Hátún, H., Counillon, F., Payne, M. R., and Visser, A. W.: Synoptic-scale
884   analysis of mechanisms driving surface chlorophyll dynamics in the North Atlantic,
885   Biogeosciences, 12, 3641-3653, https://doi.org/10.5194/bg-12-3641-2015, 2015.

886   Finck, N., Counillon, F., Bertino, L., Bouillon, S. and Rampal, P.: Validation of sea ice
887   quantities of TOPAZ for the period 1990-2010, Technical Report No. 332 of Nansen
888   Environmental and Remote Sensing Center, 2013.

889   Guemas, V., Wrigglesworth, E. B., Chevallier, M., et al.: A review on Arctic sea-ice
890   predictability and prediction on seasonal to decadal time scales. Q. J. R. Meteorolog. Soc.,
891   142(695), 546-561, https://doi.org/10.1002/qj.2401, 2014.

892   Heygster, G., Hendricks, S., Kaleschke, L., Maass, N., et al.: L-Band Radiometry for Sea-Ice
893   Applications, Final Report for ESA ESTEC Contract 21130/08/NL/EL. Institute of
894   Environmental Physics, University of Bremen, 219 pages, 2009.

895   Hibler, W. D., III: A dynamic thermodynamic sea ice model. *J. Phys. Oceanogr.*, **9,** 817–846,
896   *https://doi.org/10.1175/1520-0485(1979)009<0815:ADTSIM>2.0.CO;2*, 1979.

897   Hibler, W. D., III: Ice dynamics. chap. 9, *The Geophysics of Sea Ice,* N. Untersteiner, Ed.,
898   *NATO ASI Series B: Physics*, Plenum Press, 577–640, 1986.

899   Hunke, E. C., and Dukowicz, J. K.: An elastic-viscous-plastic model for sea ice dynamics, J.
900   Phys.   Oceanogr.,   27,   1849-1867,   https://doi.org/10.1175/1520-
901   0485(1997)027<1849:AEVPMF>2.0.CO;2, 1997.

902   Johannessen, O. M., Shalina, E. V., and Miles, M. W.: Satellite evidence for an Arctic Sea ice
903   cover in transformation, Science, 286, 1937—1939. Doi:10.1126/science.286.5446.1937,
904   1999.

905   Johannessen, J. A., et al.: Toward improved estimation of the dynamic topography and ocean
906   circulation in the high latitude and Arctic Ocean: The importance of GOCE, Surv. Geophys.,
907   35, 661–679, doi:10.1007/s10712-013-9270-y, 2014.

908   Johnson, M., Proshutinsky A., Aksenov Y., Nguyen A. T., Lindsay R., Haas C., Zhang J.,
909   Diansky N., Kwok R., et al.: Evaluation of Arctic sea ice thickness simulated by Arctic
910   Ocean Model Intercomparison Project models. J. Geophys. Res., 117(C8), C00D31,
911   doi:10.1029/2011JC007257, 2012.

912   Kaleschke, L., Maaß, N., Haas, C., Hendricks, S., Heygster, G., and Tonbøe, R.: A sea-ice
913   thickness retrieval model for 1.4 GHz radiometry and application to airborne measurements
914   over low salinity sea-ice, The Cryosphere, 4, 583-592. Doi: 10.5194/tc-4-583-2010, 2010.

915   Kaleschke, L., Tian-Kunze, X., Maaß, N., Ricker, R., Hendricks, S., and Drusch, M.: Improved
916   retrieval of sea ice thickness from SMOS and Cryosat-2. Proceedings of 2015 International
917   Geoscience   and   Remote   Sensing   Symposium   IGARSS,   doi:
918   10.1109/IGARSS.2015.7327014, 2015.

919   Karspeck, A. R.: An ensemble approach for the estimation of observational error illustrated for

a nominal 1 global ocean model. Monthly Weather Review, 144, 1713-1728, DOI: 10.1175/MWR-D-14-00336.1, 2016.

Kern, S., Khvorostovsky, K., Skourup, H., Rinne, E., Parsakhoo, Z. S., Djepa, V., Wadhams, P., and Sandven, S.: The impact of snow depth, snow density and ice density on sea ice thickness retrieval from satellite radar altimetry: results from the ESA-CCI Sea Ice ECV Project Round Robin Exercise. The Cryosphere, 9, 37-52, doi:10.5194/tc-9-37-2015, 2015.

Khvorostovsky, K., and Rampal, P.: On retrieving sea ice freeboard from ICESat laser altimeter. The Cryosphere, 10, 2329-2346, doi:10.5194/tc-10-2329-2016, 2016.

Kimmritz, M., Counillon, F., Bitz, C.M., Massonnet, F., Bethke, I. and Gao, Y., 2018. Optimising assimilation of sea ice concentration in an Earth system model with a multicategory sea ice model. *Tellus A: Dynamic Meteorology and Oceanography*, *70*(1), 1435945, https://doi.org/10.1080/1600870.2018.1435945, 2018.

King, J., Howell, S., Derksen, C., Rutter, N., Toose, P., Beckers, J. F., Haas, C., Kurtz, N., and Richter-Menge, J.: Evaluation of Operation IceBridge quick-look snow depth estimates on sea ice, Geophys. Res. Lett., 42, 9302–9310, doi:10.1002/2015GL066389, 2015.

King, J., Skourup, H., Hvidegaard, S. M., Rösel, A., Gerland, S., Spreen, G., . . . Liston, G. E. (2018). Comparison of freeboard retrieval and ice thickness calculation from ALS, ASIRAS, and CryoSat-2 in the Norwegian Arctic to field measurements made during the N-ICE2015 expedition. Journal of Geophysical Research: Oceans, 123, 1123–1141. https://doi.org/10.1002/ 2017JC013233

Kinnard, C., Zdanowicz, C. M., Fisher, D. A., Isaksson, E., Vernal, A., and Thompson, L. G.: Reconstructed changes in Arctic sea ice over the past 1,450 years. Nature, 479, 509– 512. doi:10.1038/nature10581, 2011.

Kwok, R., and Rothrock, D.: Decline in Arctic sea ice thickness from submarine and ICESat records: 1958–2008, Geophys. Res. Lett., 36, L15501, doi:10.1029/2009GL039035, 2009.

Kurtz, N. T., Farrell, S. L., Studinger, M., Galin, N., Harbeck, J. P., Lindsay, R., Onana, V. D., Panzer, B., and Sonntag, J. G.: Sea ice thickness, freeboard, and snow depth products from Operation IceBridge airborne data, The Cryosphere, 7, 1035-1056, doi:10.5194/tc-7-1035-2013, 2013.

Laxon, S., Peacock, N., and Smith, D.: High interannual variability of sea ice thickness in the Arctic region, Nature, 425, 947-950, doi:10.1038/nature02050, 2003.

Lavergne, T., Eastwood, S., Teffah, Z., Schyberg, H., and Breivik, L. -A.: Sea ice motion from low resolution satellite sensors: an alternative method and its validation in the Arctic. *Journal of Geophysical Research*, 115, C10032, 2010. doi: 10.1029/2009JC005958, 2010.

954   Levermann, A., Mignot, J., Nawrath, S., Rahmstorf, S.: The role of Northern sea ice cover for

955   the weakening of the thermohaline circulation under global warming. J. Climate, 20, 4160-

956   4171, *https://doi.org/10.1175/JCLI4232.1*, 2007.

957   Lindsay, R., and Schweiger, A.: Arctic sea ice thickness loss determined using subsurface,

958   aircraft, and satellite observations, The Cryosphere, 9, 269-283, dos:10.5194/tc-9-269-2015,

959   2015.

960   Lisæter, K. A., Rosanova, J. J., and Evensen, G.: Assimilation of ice concentration in a coupled

961   ice ocean model, using the Ensemble Kalman filter. Ocean Dynamics, 53, 368-388,

962   doi:10.1007/s10236-003-0049-4, 2003.

963   Lisæter, K. A., Evensen, G., and Laxon, S.: Assimilating synthetic CryoSat sea ice thickness in

964   a coupled ice-ocean model, J. Geophys. Res., 112, C07023, doi:10.1029/2006JC003786,

965   2007.

966   Martin, S., Drucker, R., Kwok, R., and Holt, B.: Estimation of the thin ice thickness and heat

967   flux for the Chukchi Sea Alaskan coast polynya from Special Sensor Microwave/Imager

968   data, 1990-2001, J. Geophys. Res., 109, C10012, https://doi.org/10.1029/2004JC002428,

969   2004.

970   Massonnet, F., Goosse, H., Fichefet, T., and Counillon, F.: Calibration of sea ice dynamic

971   parameters in an ocean-sea ice model using an ensemble Kalman filter, J. Geophys. Res.,

972   119(7), 4168-4184, https://doi.org/10.1002/2013JC009705, 2014.

973   Mathiot, P., König Beatty, C., Fichefet, T., Goosse, H., Massonnet, F., and Vancoppenolle, M.:

974   Better constraints on the sea-ice state using global sea-ice data assimilation, Geosci. Model

975   Dev., 5, 1501-1515, https://doi.org/10.5194/gmd-5-1501-2012, 2012.

976   Melia, N., Haines, K., and Hawkins, E.: Improved Arctic sea ice thickness projections using

977   bias-corrected   CMIP5   simulations,   The   Cryosphere,   9,   2237-2251,

978   https://doi.org/10.5194/tc-9-2237-2015, 2015.

979   Metzger, E. J., Smedstad, O. M., Thoppil, P. G., Hurlburt, H. E., Cummings, J. A., Wallcraft,

980   A. J., Zamudio, L., Franklin, D. S., Posey, P. G., Phelps, M. W. and Hogan, P. J.: US Navy

981   operational global ocean and Arctic ice prediction systems. *Oceanography*, *27*(3), 32-43,

982   https://doi.org/10.5670/oceanog.2014.66, 2014.

983   Mu, L., Yang, Q., Losch, M., Losa, S. N., Ricker, R., Nerger, L., and Liang, X.: Improving sea

984   ice thickness estimates by assimilating CryoSat-2 and SMOS sea ice thickness data

985   simultaneously. Q. J. R. Meteorol. Soc., 144(711), 529-538, DOI:10.1002/qj.3225, 2018.

986   Oke, P. R., and Sakov, P.: Representation error of oceanic observations for data assimilation.

987   J. Atmos. Oceanic Technol., 25, 1004–1017, doi:10.1175/2007JTECHO558.1, 2008.

Oki, T., and Sud, Y. C.: Design of Total Runoff Integrating Pathways (TRIP)—A Global River Channel Network. *Earth Interact.*, **2**, 1–37, https://doi.org/10.1175/1087-3562(1998)002<0001:DOTRIP>2.3.CO;2, 1998.

Olason, E., and Notz, D.: Drivers of variability in Arctic sea-ice drift speed, J. Geophys. Res. Oceans, 119,5755–5775, doi:10.1002/2014JC009897, 2014.

Penny, G., Akella, S.R., Frolov, S., Fujii, Y., Karspeck, A., Peña, M., Subramanian, A., Tardif, R., Wu, X., Anderson, J., Kalnay, E., Kleist, D.T., and Todling, R.: Coupled Data Assimilation for Integrated Earth System Analysis and Prediction : Goals , Challenges , and Recommendations. Technical Report, https://ntrs.nasa.gov/search.jsp?R=20170007430, 2017.

Perovich, D. K., and Richter-Menge, J. A.: From points to Poles: extrapolating point measurements of sea-ice mass balance. *Ann. Glaciol.*, **44**, 188–192, doi:10.3189/172756406781811204, 2006.

Posey, P. G., Metzger, E. J., Wallcraft, A. J., Hebert, D. A., Allard, R. A., Smedstad, O. M., Phelps, M. W., Fetterer, F., Stewart, J. S., Meier, W. N., and Helfrich, S. R.: Improving Arctic sea ice edge forecasts by assimilating high horizontal resolution sea ice concentration data into the US Navy's ice forecast systems, The Cryosphere, 9, 1735-1745, dos:10.5194/tc-9-1735-2015, 2015.

Rampal, P., J. Weiss, and D. Marsan, 2009: Positive trend in the mean speed and deformation rate of Arctic sea ice, 1979-2007, J. Geophys. R., 114(C5), doi:10.1029/2008JC005066.

Rampal, P., Bouillon, S., Ólason, E., and Morlighem, M.: neXtSIM: a new Lagrangian sea ice model. *The Cryosphere*, *10*(3), 1055–1073, 2016.

Ricker, R., Hendricks, S., Helm, V., Skourup, H., and Davidson, M., Sensitivity of CryoSat-2 Arctic sea-ice freeboard and thickness on radar-waveform interpretation, The Cryosphere, 8, 1607-1622, doi:10.5194/tc-8-1607-2014, 2014.

Ricker, R., Hendricks, S., Kaleschke, L., Tian-Kunze, X., King, J. and Haas, C.: A weekly Arctic sea-ice thickness data record from merged CryoSat-2 and SMOS satellite data, The Cryosphere, 11, 1607-1623, doi:10.5194/tc-11-1607-2017, 2017.

Rodgers, C.: Inverse methods for atmospheres: theory and practice, World Scientific, 2000.

Rodwell, M. J., Lang, S. T. K., Ingleby, N. B., Bormann, N., Hólm, E., Rabier, F., Richardson, D. S. and Yamaguchi, M.: Reliability in ensemble data assimilation. Quart. J. Roy. Meteor. Soc., 142, 443–454, doi: 10.1002/qj.2663, 2016.

Sakov, P., and Oke, P. R.: A deterministic formulation of the ensemble Kalman Filter: an alternative to ensemble square root filters. Tellus A, 60(2), 361-371, doi:10.1111/j.1600-0870.2007.00299.x, 2008.

1023   Sakov, P., Counillon, F., Bertino, L., Lisæter, K. A., Oke, P. R., and Korablev, A.: TOPAZ4:

1024   an ocean-sea ice data assimilation system for the North Atlantic and Arctic. *Ocean Science*,

1025   8(4), 633–656. http://doi.org/10.5194/os-8-633-2012, 2012.

1026   Schofield, O., Ducklow, H. W., Martinson, D. G., Meredith, M. P., Moline, M. A., and Fraser,

1027   W. R.: How Do Polar Marine Ecosystems Respond to Rapid Climate Change? Science

1028   (328), 5985, 1520–1523, DOI: 10.1126/science.1185779, 2011.

1029   Schweiger, A., Lindsay, R., Zhang, J., Steels, M., Stern, H., and Kwok, R.: Uncertainty in

1030   modeled Arctic sea ice volume, J. Geophys. R., 116, C00D06, doi:10.1029/2011JC007084,

1031   2012.

1032   Smith, G. C., Roy, F., Reszka, M., Colan, D. S., He, Z., Deacu, D., et al.: Sea ice forecast

1033   verification in the Canadian Global Ice Ocean Prediction System. Quart. J. Roy. Meteor.

1034   Soc., doi:10.1003/qj.2555, 2015.

1035   Stark, J. D., J. Ridley, M. Martin, M., and Hines, A.: Sea ice concentration and motion

1036   assimilation in a sea ice–ocean model, J. Geophys. Res., 113, C05S91,

1037   doi:10.1029/2007JC004224, 2008.

1038   Stonebridge, G., Scott, K. A., and Buehner, M.: Impacts on sea ice analyses from the

1039   assumption of uncorrelated ice thickness observation errors: Experiments using a 1D toy

1040   model, Tellus A: Dynamic Meteorology and Oceanography, 70(1), 1445379, DOI:

1041   10.1080/16000870.2018.1445379, 2018.

1042   Stroeve, J. C., Serreze, M. C., Holland, M. M. et al.: The Arctic's rapidly shrinking sea ice

1043   cover: a research synthesis. Climatic change, 10 (3), 1005-1027, doi:10.1007/s10584-011-

1044   0101-1, 2012.

1045   Sumata, H., Lavergne, T., Girard-Ardhuin, F., Kimura, N., Tschudi, M. A., Kauker, F., Karcher,

1046   M., and Gerdes, R.: An intercomparison of Arctic ice drift products to deduce uncertainty

1047   estimates, J. Geophys. Res. Oceans, 119, 4887–4921, doi:10.1002/ 2013JC009724, 2014.

1048   Tian-Kunze, X., Kaleschke, L., Maaß, N., Mäkynen, M., Serra, N., Drusch, M., and Krumpen,

1049   T.: SMOS-derived sea ice thickness: algorithm baseline, product specifications and initial

1050   verification, The Cryosphere, 8, 997-1018, doi:10.5194/tc-8-997-2014, 2014.

1051   Tilling, R. L., Ridout, A., and Shepherd, A.: Near real time Arctic sea ice thickness and volume

1052   from CryoSat-2, The Cryosphere, 10, 2003-2012, doi:10.5194/tc-10-2003-2016, 2016.

1053   Tilling, R. L., Ridout, A., and Sheperd, A.: Estimating Arctic sea ice thickness and volume

1054   using CryoSat-2 radar altimeter data. *Advances in Space Research*, 62(6), 1203-1225,

1055   http://doi.org/10.1016/j.asr.2017.10.051, 2018.

1056   Uotila, P., Goosse, H., Haines, K., Chevallier, M., Barthélemy, A., Bricaud, C., Carton, J.,

1057   Fučkar, N., Garric, G., Iovino, D., Kauker, F., Korhonen, M., Lien, V. S., Marnela, M.,

1058   Massonnet, F., Mignac, D., Peterson, A., Sadikn, R., Shi, L., Tietsche, S., Toyoda, T., Xie,
1059   J., Zhang, Z.: An assessment of ten ocean reanalyses in the polar regions, Climate Dynamics,
1060   https://doi.org/10.1007/s00382-018-4242-z, 2018.

1061   Wang, Q., Ilicak, M., Gerdes, R., Drange, H., Aksenov, Y., Bailey, D. A., … Yeager, S. G. An
1062   assessment of the Arctic Ocean in a suite of interannual CORE-II simulations. Part I: Sea
1063   ice and solid freshwater. *Ocean Modelling*, *99*, 110–132.
1064   http://doi.org/10.1016/J.OCEMOD.2015.12.008, 2016a

1065   Wang, X., Key, J., Kwok, R., and Zhang, J.: Comparison of Arctic sea ice thickness from
1066   satellites, aircraft, and PIOMAS data. *Remote Sensing*, *8*(9), 1–17,
1067   http://doi.org/10.3390/rs8090713, 2016b.

1068   Woodgate, R., Aagaard, K. and Weingartner, T.: Monthly temperature, salinity, and transport
1069   variability of the Bering Strait through flow. *Geophys*. *Res*. *Lett*., 32, L04601, DOI:
1070   10.1029/2004GL021880, 2005.

1071   Xie, J., Bertino, L., Counillon, F., Lisæter, K. A., and Sakov, P.: Quality assessment of the
1072   TOPAZ4 reanalysis in the Arctic over the period 1991–2013. *Ocean Science*, 13(1), 123–
1073   144. http://doi.org/10.5194/os-13-123-2017, 2017.

1074   Xie, J., Bertino, L., Cardellach, E., Semmling, M., and Wickert, J.: An OSSE evaluation of the
1075   GNSS-R altimetery data for the GEROS-ISS mission as a complement to the existing
1076   observational networks, *Remote Sens*. *Environ*., 209, 152-165,
1077   doi:10.1016/j.rse.2018.02.053, 2018.

1078   Xie, J., Counillon, F., Bertino, L., Tian-Kunze, X., and Kaleschke, L.: Benefits of assimilating
1079   thin sea-ice thickness from SMOS into the TOPAZ system. *The Cryosphere*, 10, 2745–2761.
1080   http://doi.org/10.5194/tc-10-2745-2016, 2016.

1081   Yang, Q., Losa, S. N., Losch, M., Tian-Kunze, X., Nerger, L., Liu, J., Kaleschke, L., and Zhang,
1082   Z.: Assimilating SMOS sea ice thickness into a coupled ice-ocean model using a local SEIK
1083   filter, J. Geophys. Res., 119, 6680–6692, doi:10.1002/2014JC009963, 2014.

1084

Figures:
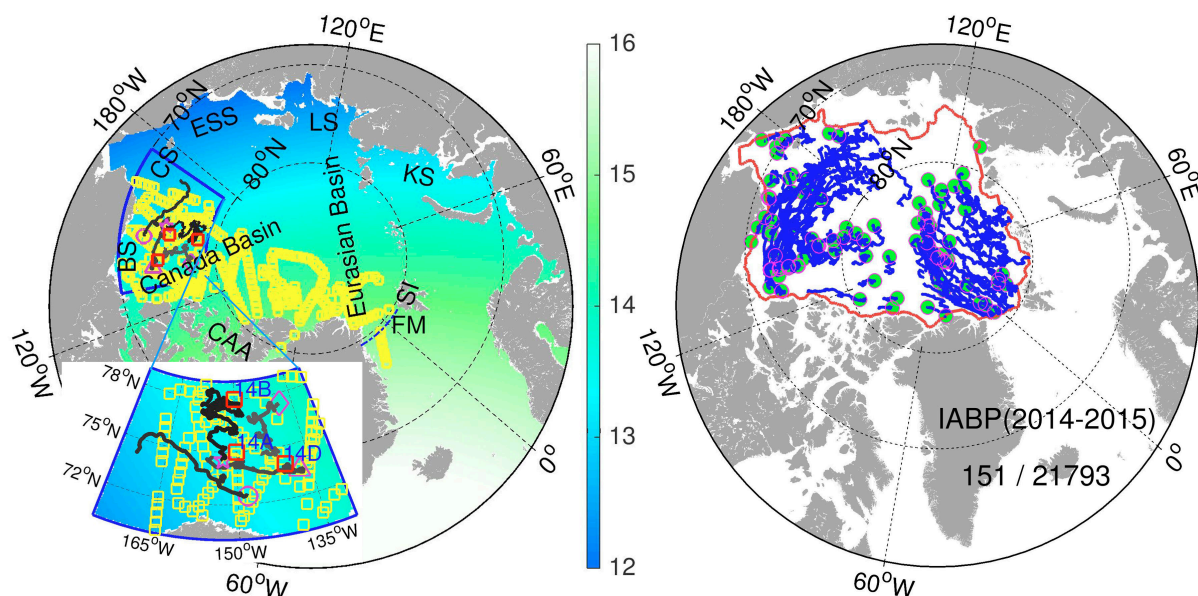
Fig. 1 Left: Horizontal resolution (km) of the model grid in the Arctic (>60°N). The small yellow squares are the locations of IceBridge campaigns during the experimental period. The marginal seas are: Beaufort Sea (BS, ; also shown with the blue line), Chukchi Sea (CS), East Siberian Sea (ESS), Laptev Sea (LS), Kara Sea (KS) and the other regions: Canadian Arctic Archipelago (CAA), Svalbard Island (SI), and Fram Strait (FM). The four purple markers (star, circle, triangle and diamond) are the deployment location of IMB buoys (2013F, 2014B, 2014C, and 2014F respectively) with the following trajectory shown as black solid curves. The three red squares are the fixed locations of the BGEP moorings (14A, 14B, and 14D respectively). **Right**: Trajectories of International Arctic Buoy Program buoys drift during the experimental period. The solid red line delimits the coastal areas excluded in the analysis.

1107

1108

1109 **Fig**. **2** Observation error uncertainties as a function of sea ice thickness for the
1110 original CS2SMOS data set (black line), the estimated observation error using the
1111 Desroziers diagnostics with red-triangle line (see Eq. (3)) and the one used in the
1112 TOPAZ Test run with blue-square, with an additional error term as Eq. (4) to the
1113 original uncertainty.
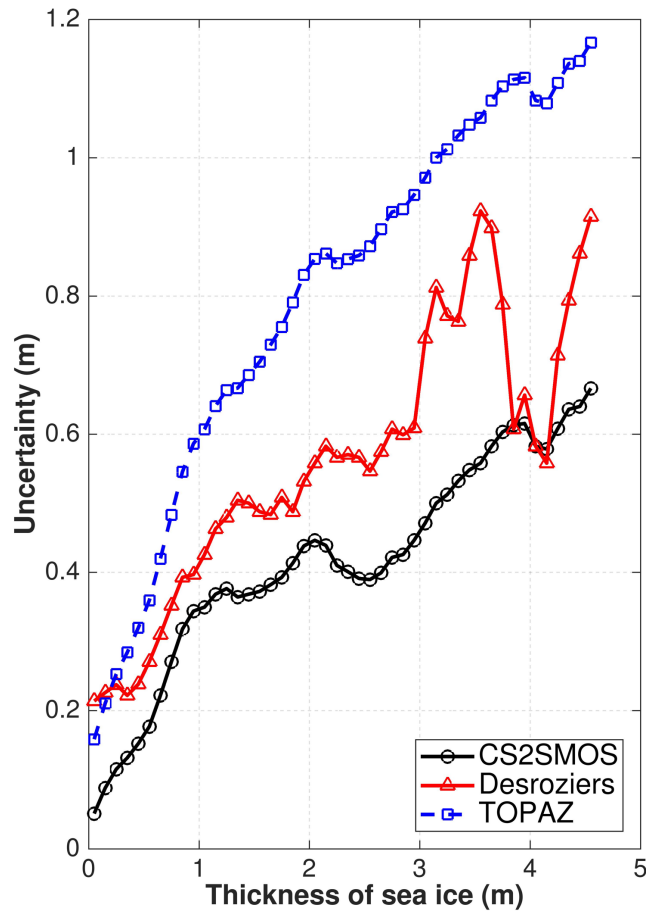
1114

1115

1116

1117

1118

1119

1120

1121

1122

1123   0

1124

1125
1126
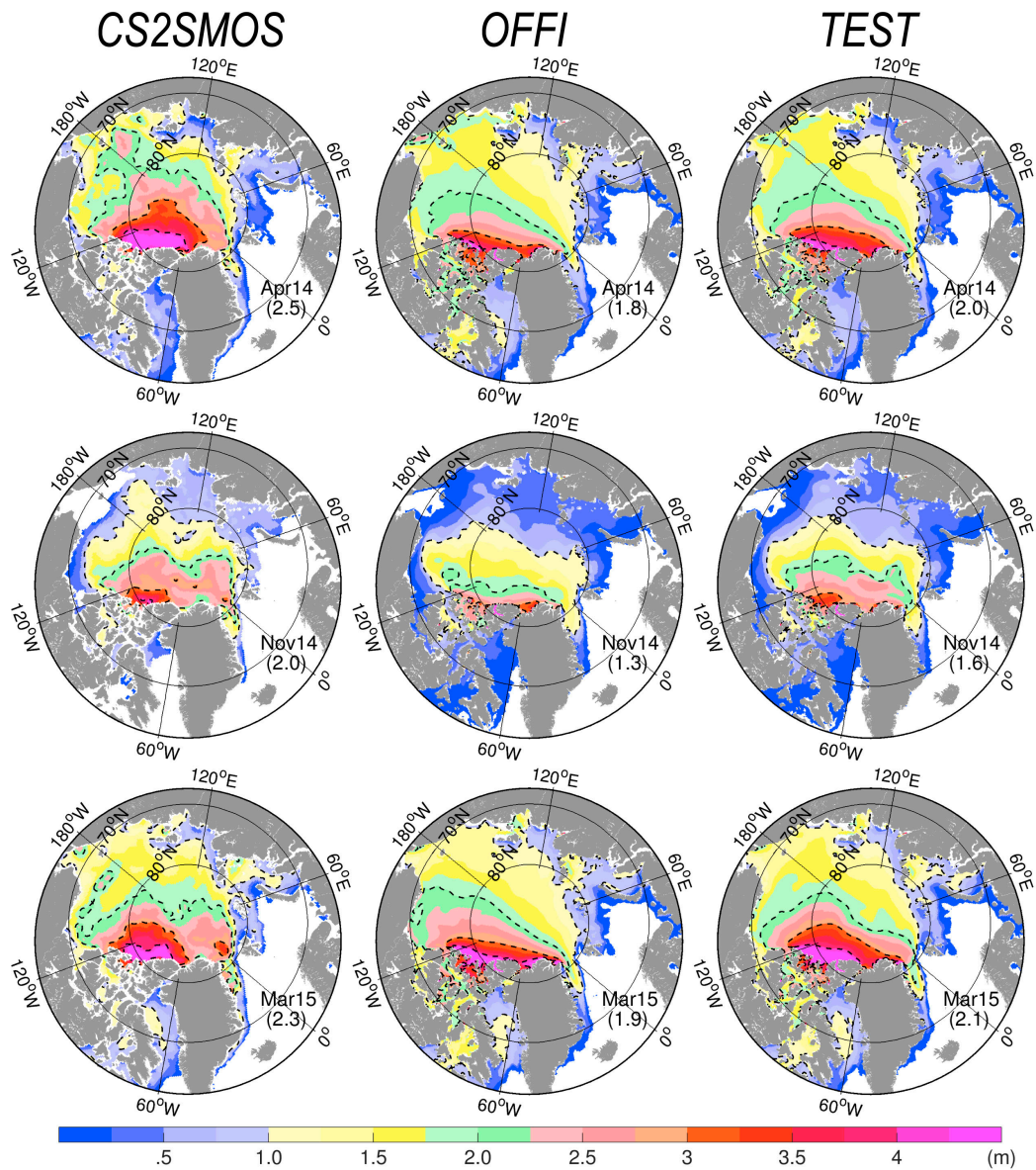
1127 **Fig**. **3** Monthly SIT from CS2SMOS (left), Official run (middle) and Test run (right) in

1128 April 2014, November 2014, and March 2015. The mean SIT estimated for the area

1129 north of 80N is indicated in brackets (unit: m). The dashed lines are isolines of 1, 2,

1130 3, and 4 meters SIT respectively.

1131
1132
1133
1134
1135
1136
1137

1138

1139
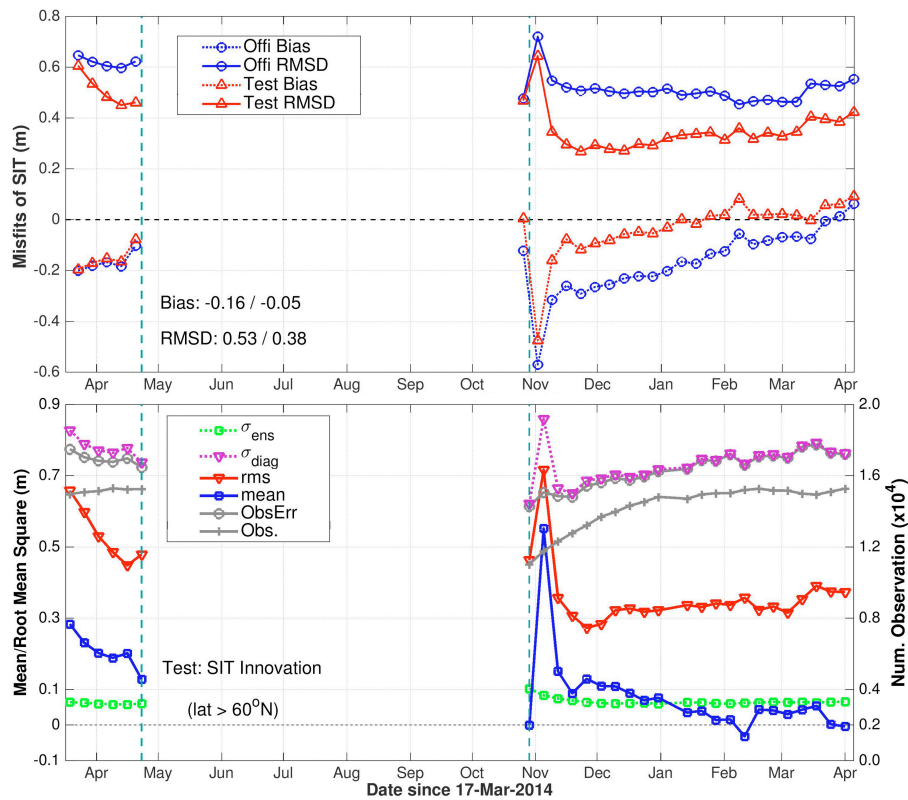
1140 **Fig**. **4 Top**: Bias (dotted line) and RMSD (solid line) of SIT in the two runs - Official

1141 (blue) and Test (red) – based on weekly averaged reanalysis and CS2SMOS

1142 observations. The time-averaged bias and RMSD are indicated (Official/Test).

1143 **Bottom**: SIT innovation statistics in the Test run in the Arctic region (>60°N) from

1144 19th March 2014 to end of March 2015. The blue-squared (resp. red reverted-triangle)

1145 line represents the mean (RMSD) of the innovation. The green squared line

1146 represents the ensemble spread and the purple reverted-triangle line is the

1147 diagnosed total uncertainty (see Eq. (8)). The gray-crossed (gray-circled) line is the

1148 number (RMSD observation error) of assimilated observations.

1149

1150

1151

1152

1153

1154

1155

1156

1157

1158
1159
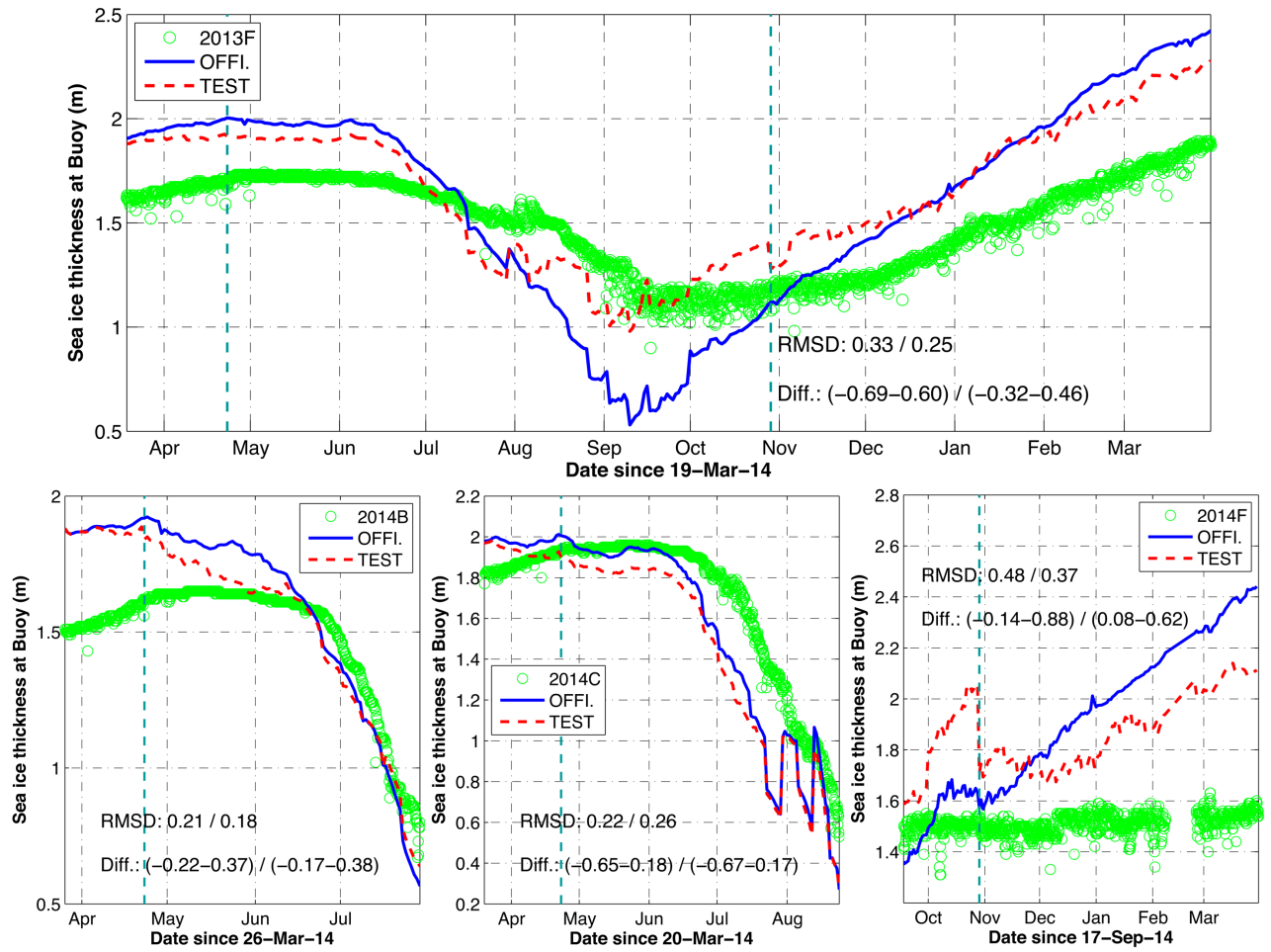
1160   **Fig**. **5** Time series of SIT along the trajectories of IMB buoys (upper: 2013F; bottom:

1161   2014B, 2014C, and 2014F). Measured SIT (green), daily averages from the Official

1162   run (blue line) and the Test run (red line). The vertical cyan-dashed lines indicate

1163   the winter period when C2SMOS is assimilated in the Test run.

1164
1165
1166
1167
1168
1169
1170
1171
1172
1173

1174
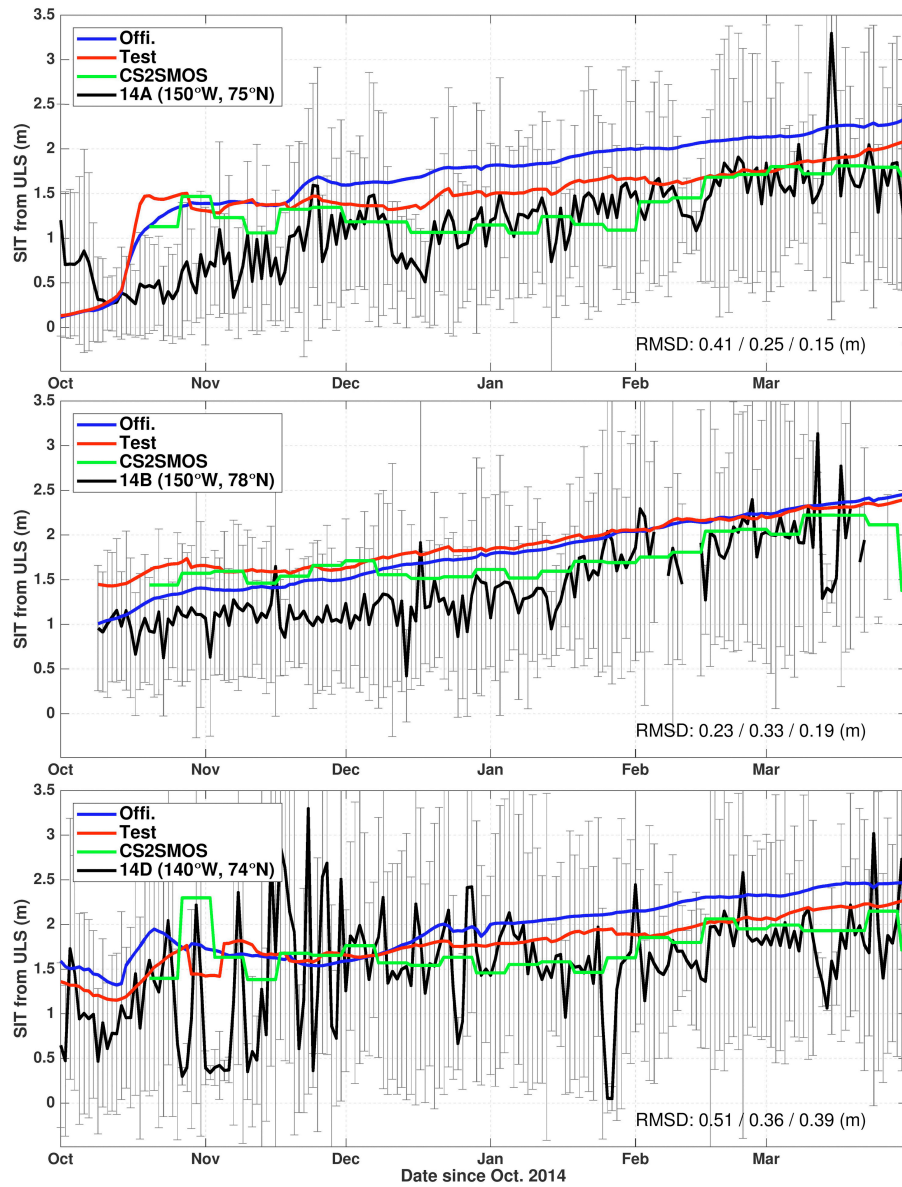
1175 **Fig**. 6 Daily series of SIT (black line) at the BGEP mooring (14A, 14B, and 14D)

1176 compared with the two model runs - Official (blue line) and Test (red line) - and

1177 the weekly observed by CS2SMOS (green line). The black line represents the

1178 daily average at the mooring location with the standard deviation shown as the

1179 error bar. The RMSDs of the Official run, Test run and CS2SMOS are

1180 respectively indicated on the bottom of each panels.

1181

1182

1183

1184

1185

1186
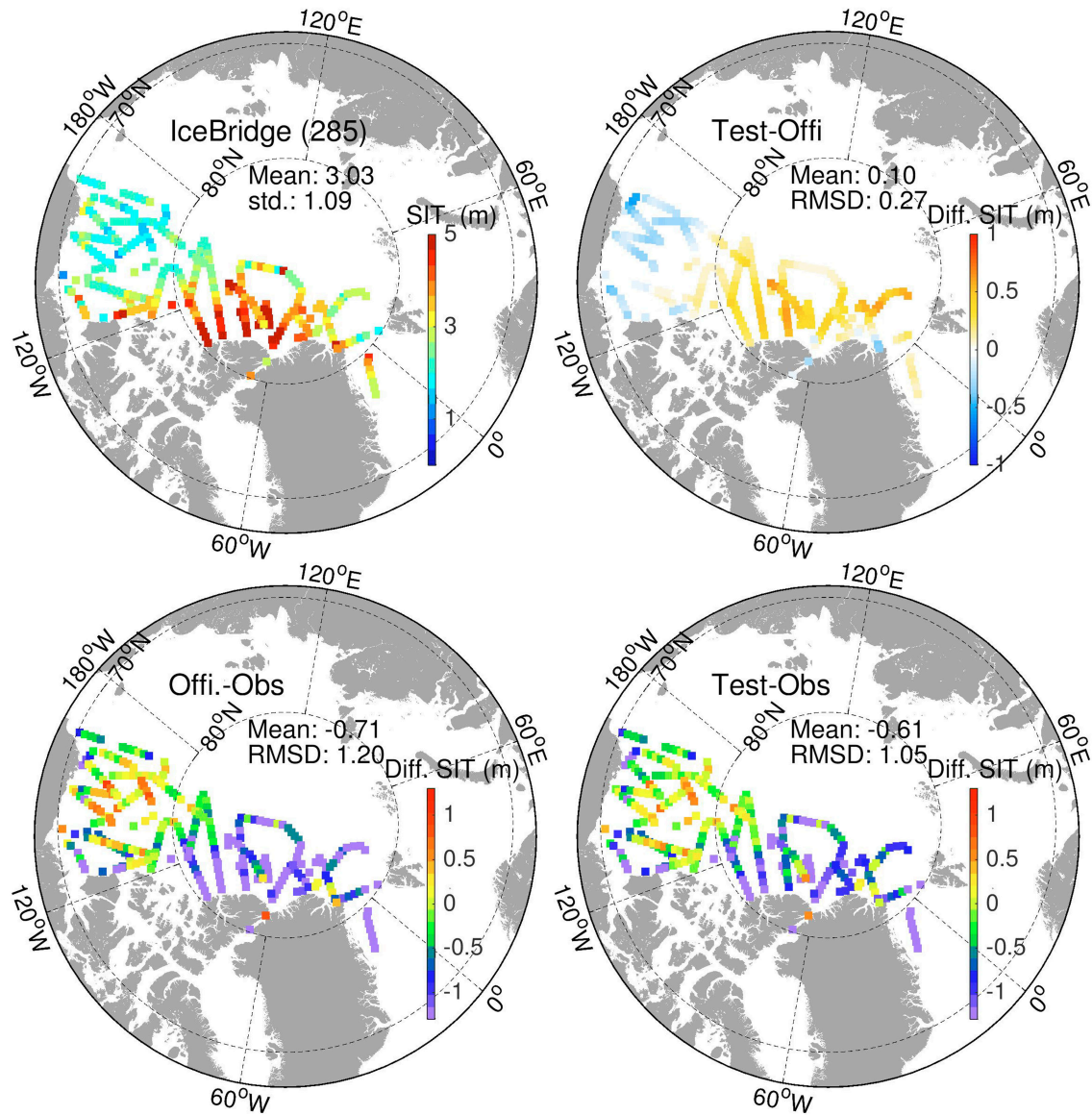
1187 **Fig**. **7 Top**: IceBridge SIT in 2014 and 2015 (left) and the SIT differences in the two

1188 model runs according to the observational locations and times (right). **Bottom**: SIT

1189 deviations from the Official run (left) and Test run (right) using model daily average

1190 at observations time.

1191

1192

1193

1194

1195

1196

1197

1198

1199

1200

1201

1202

1203

1204

1205
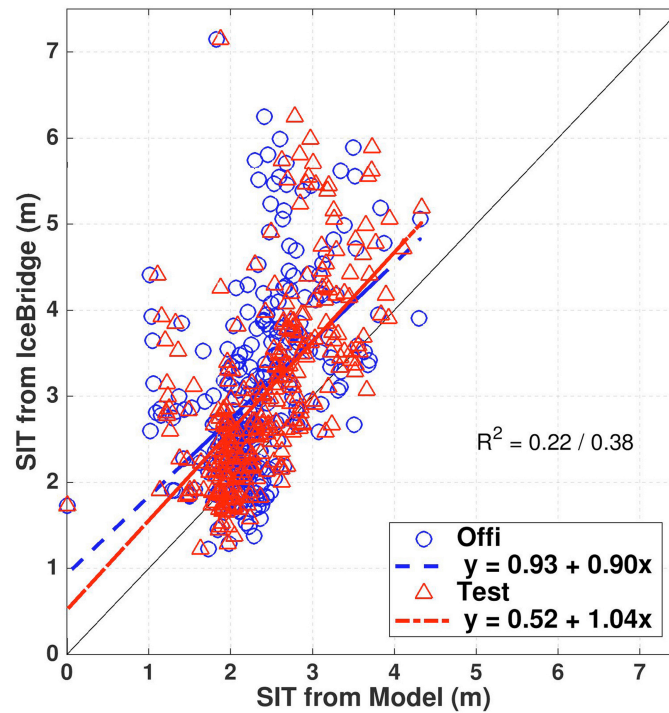
1206 **Fig**. **8** Scatterplots of SIT daily averaged of Official (blue) and Test (red) runs

1207 compared to IceBridge data. The dashed lines are the respective linear regression,

1208 the coefficient R^2 is the squared correlation to represent how strong of the linear

1209 relationship in Official/Test run. The black line is y=x.

1210

1211

1212

1213

1214

1215

1216

1217

1218

1219

1220
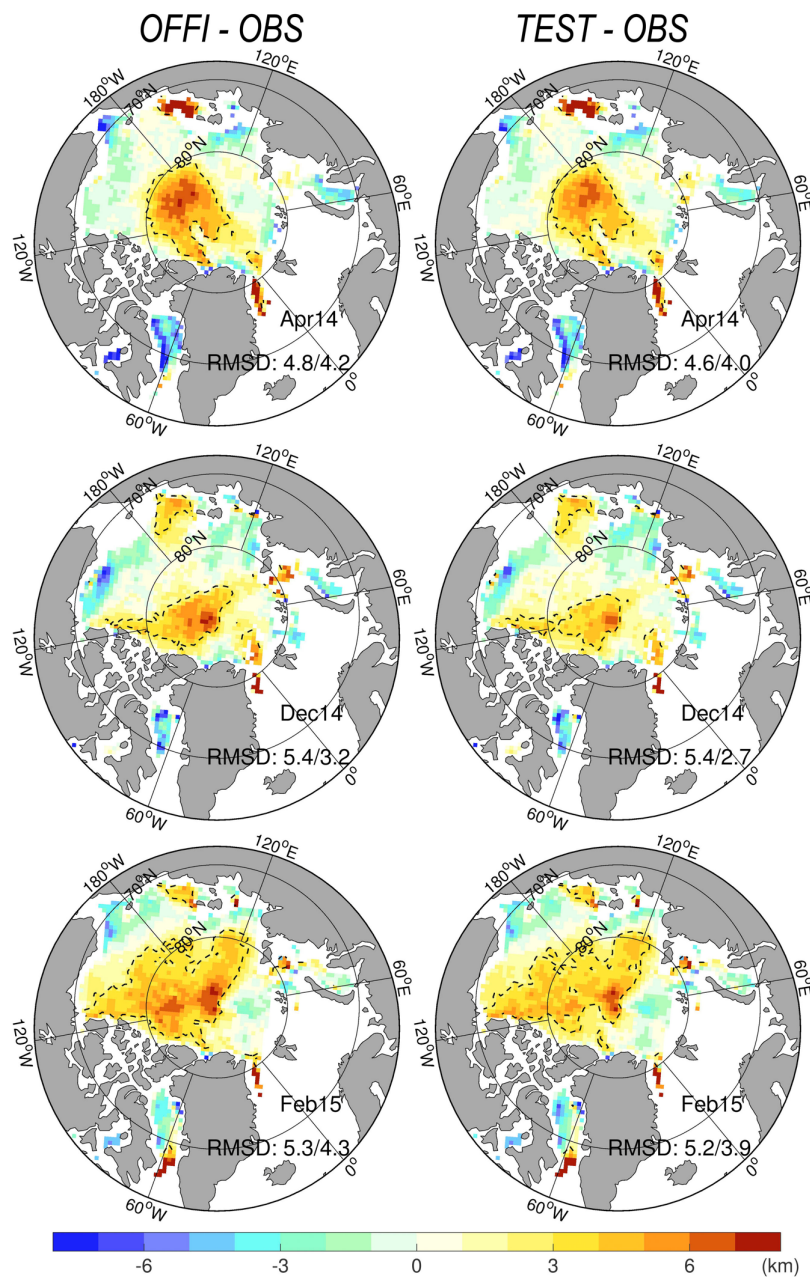
1221

1222 **Fig**. **9** Sea ice drift misfits (model minus observation, in km per two days) in the
1223 Official run (left column) and Test run (right column) compared against the OSI-SAF
1224 sea ice drift in April 2014 (top line), December 2014 (middle line), and February 2015
1225 (bottom line). The black dashed delimits the area of fastest drift (drift > 3km per 2
1226 days), and the RMSD relative to the monthly observations is indicated when
1227 calculated for the whole domain and at for the region north of 80°N.

1228

1229

1230

1231

1232

1233
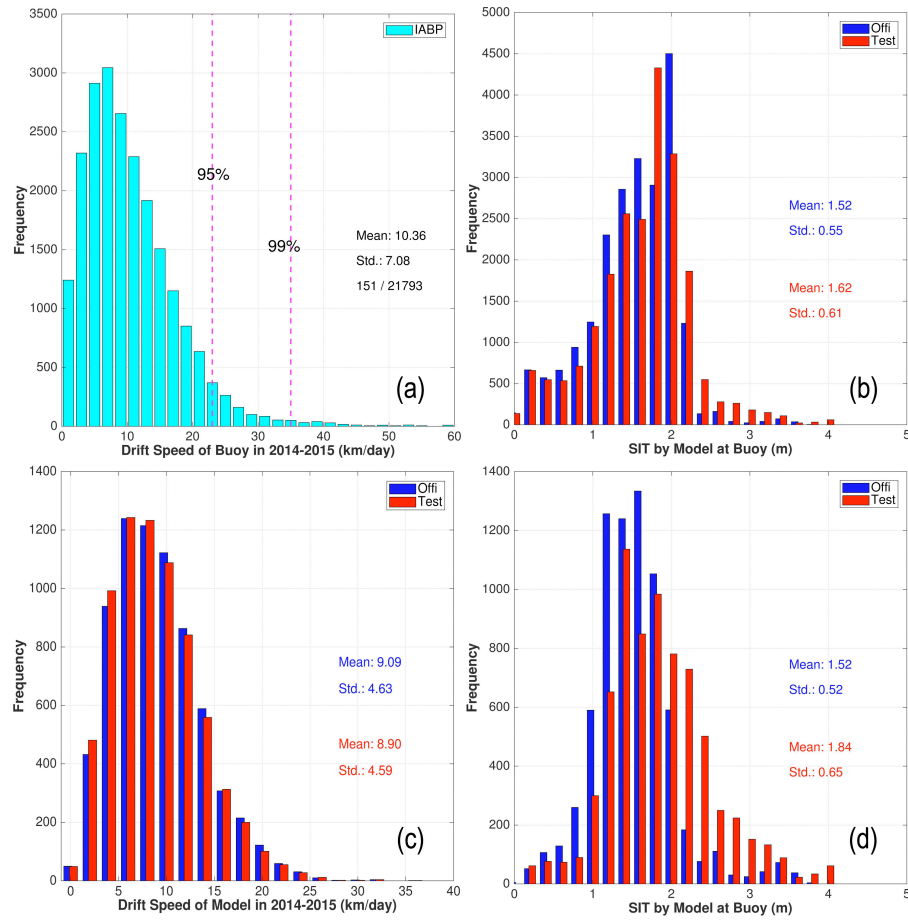
1234 **Fig**. **10** (a) Histogram of sea ice drift speeds calculated from IABP buoys in the

1235 central Arctic for the period 2014-2015. (b) histogram of the simulated SIT at buoys

1236 locations in the central Arctic from the two runs. (c) histogram of the drift speed

1237 restricted near the North pole (>80°N) in the Official (blue) and Test (red) runs; the

1238 mean speed and the standard deviation are indicated; (d) histogram of the simulated

1239 SIT near the North pole from the two runs;

1240

1241

1242

1243
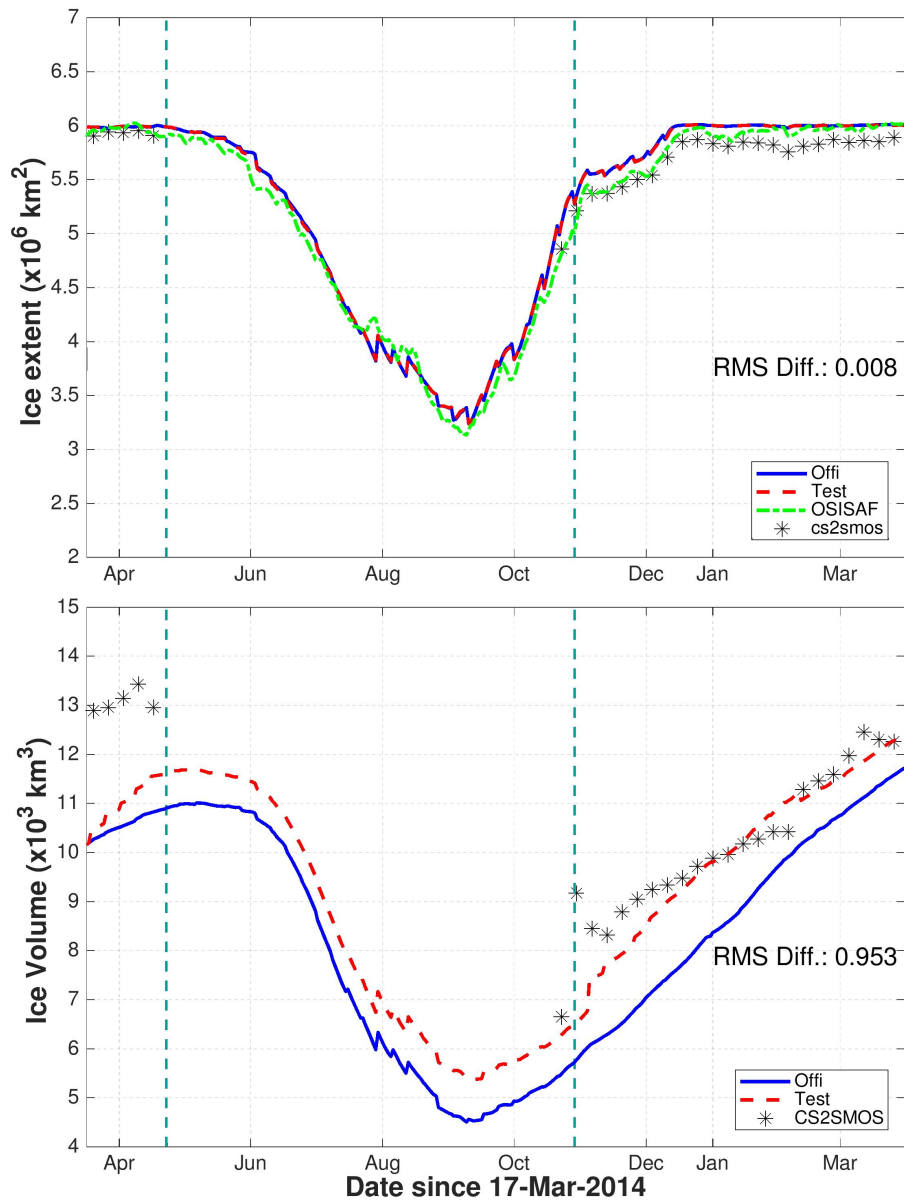
Fig. **11** SIE and SIV in the official run (blue) and the test run (red) in the Central
Arctic. The black stars are the corresponding weekly SIE (or SIV) estimated from
CS2SMOS. The green dash-dotted line is the daily SIE from OSI-SAF. The
averaged differences of the two runs (Official-Test) are reported. The vertical cyan-
dashes delimits the periods when C2SMOS data is assimilated.

1244
1245
1246
1247
1248
1249
1250
1251
1252
1253
1254
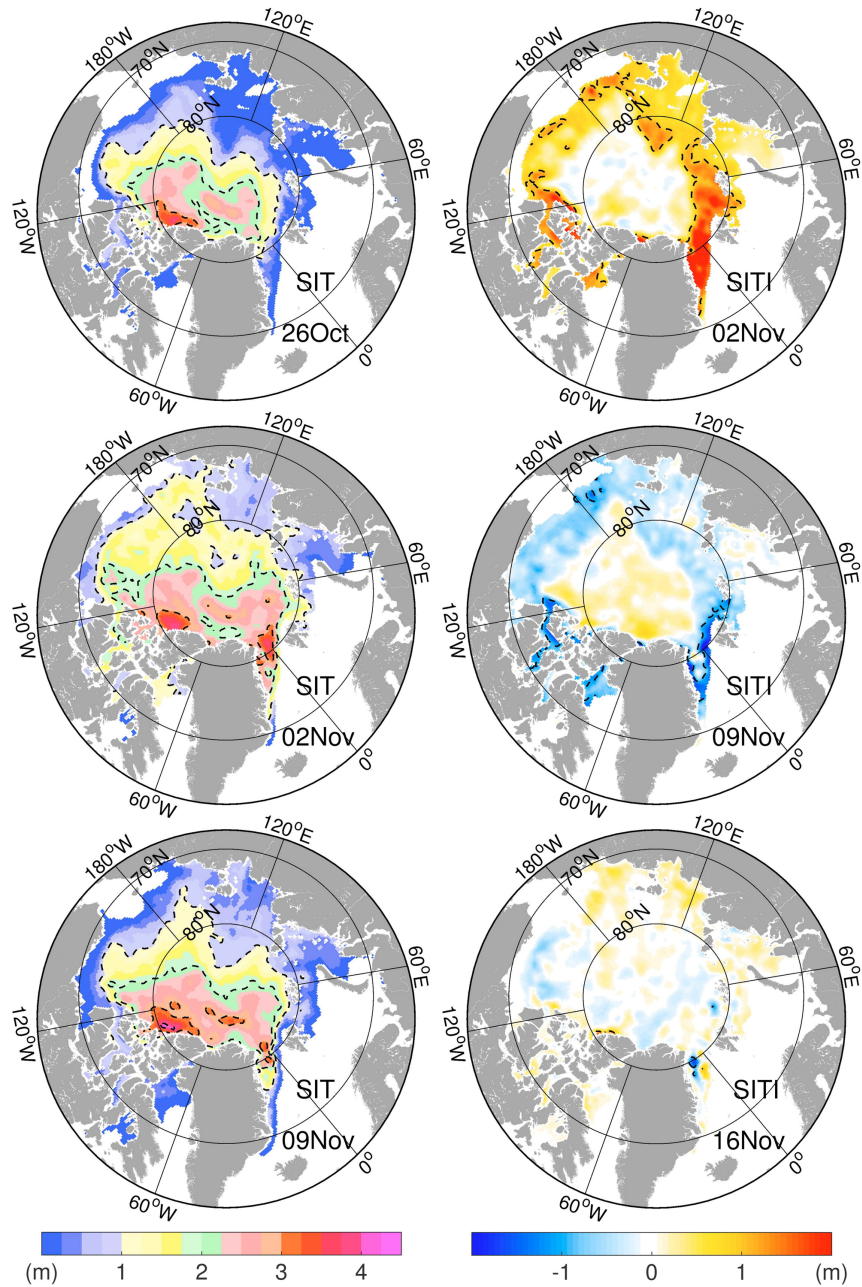
Fig. **12 Left**: First three weekly SITs (20th-26th Oct; 27th Oct-2nd Nov; 3rd-9th Nov)
from CS2SMOS in the beginning of fall 2014. The dashed white lines denote
the 1, 2, 3, and 4 m isolines. **Right**: The associated time increments of SIT
relative to the last weekly SIT. The dashed lines denote the -1 and 1 m isolines.

1265
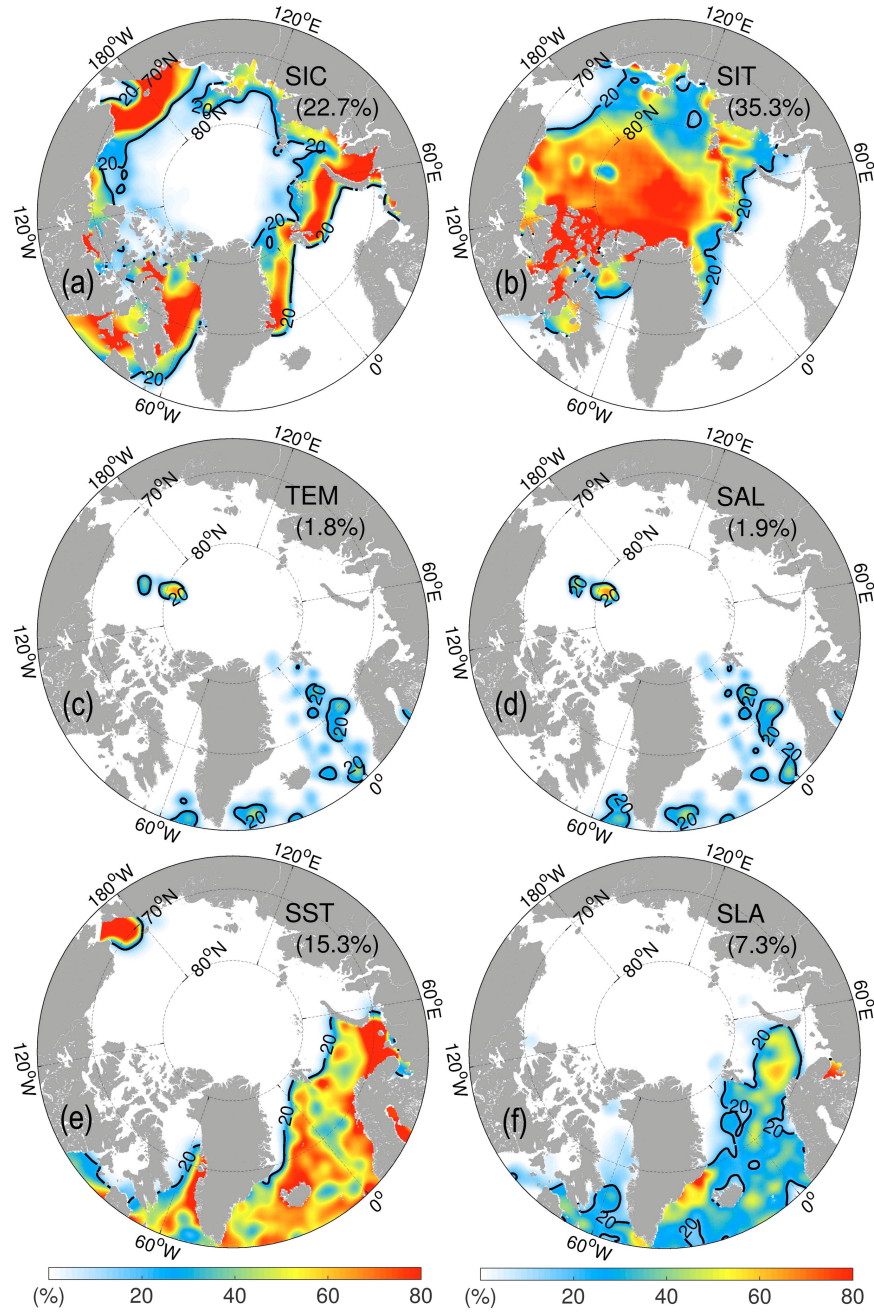
1266 **Fig**. **13** Relative DFS contributions (IF) of each observation data types in November

1267 2014. (a) SIC from OSI-SAF; (b) SIT from CS2SMOS; (c) temperature profiles; (d)

1268 salinity profiles; (e) SST; (f) along-track sea level anomaly (SLA). The black line is

1269 the 20% isoline, and the monthly IF (see Eq. 15) is reported between parenthesis.

1270

1271

1272

1273

1274

1275
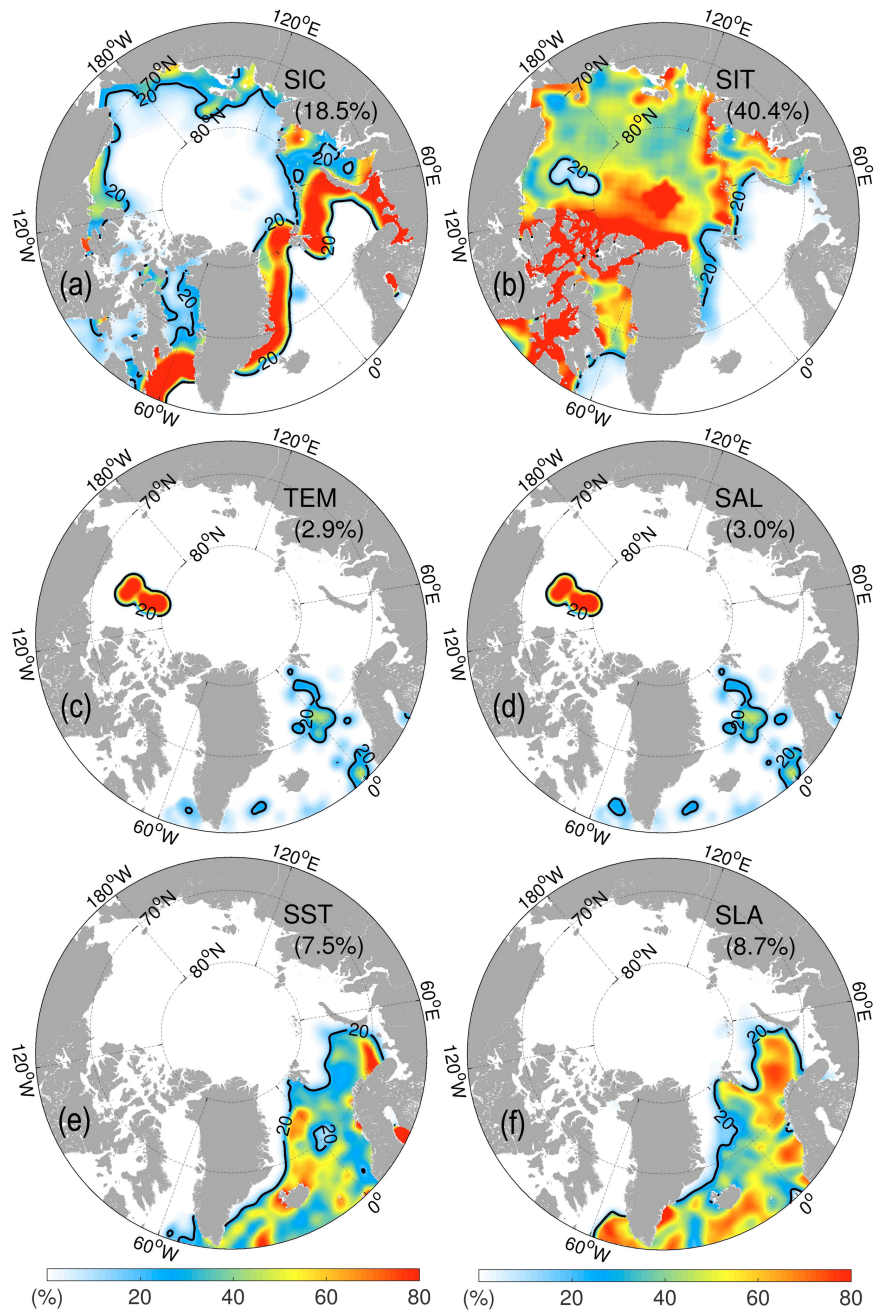
1276 **Fig**. **14** Same as the above but for March 2015.

1277

1278

1279